The JPL Extragalactic Radio Reference Frame: Astrometric Results of 1978–96 Deep Space Network VLBI

C. S. Jacobs,[1] O. J. Sovers,[1] C. J. Naudet,[1] R. F. Coker,[2] and R. P. Branson[3]

Celestial reference frames determined from measurements of extragalactic radio sources are used in interplanetary navigation, Earth orientation measurements, geodesy, and astrometry. The JPL 1997-3 celestial reference frame is derived from very long baseline interferometric (VLBI) measurements of 291 compact extragalactic radio sources. The observations were done principally at 8.4 GHz, supplemented by simultaneous 2.3-GHz observations needed to calibrate the charged-particle effects of the solar plasma and the Earth's ionosphere. The radio source positions that constitute this frame have median formal precisions of 123 and 188 microarcseconds (μas) in $\alpha \cos\delta$ and δ, respectively. Within the presently available 17.5-year span of observations, these sources are characterized by coordinate drifts that have median uncertainties of approximately 70 μas/yr. Only a few of these rates are statistically significant, and they probably are caused by variations in the internal structure of the sources. In agreement with the general relativistic theory of gravity, the parameterized post-Newtonian $\gamma_{\rm PPN}$ factor is determined to be $\gamma_{\rm PPN} = 1.001 \pm 0.001$. On the basis of internal consistency tests and comparisons to independent celestial frame determinations, we estimate that the formal uncertainties must be increased by a factor of 2 in order to more realistically describe the accuracy of the source positions. The dominant error comes from inaccurate modeling of the troposphere and, to lesser extents, from the lack of radio source structure models and imperfectly calibrated instrumentation. We briefly describe models of the observation covariances caused by these classes of errors and assess the size of remaining unmodeled errors. The absence of an all Southern-Hemisphere baseline makes the positions of southern sources especially sensitive to tropospheric mismodeling. As a result, zonal errors in the south may approach 1 milliarcsecond. The JPL frame provides an important independent verification of the International Astronomical Union's (IAU's) new International Celestial Reference Frame at the level of a few hundred μas. Finally, we review the work done to link the VLBI extragalactic radio frame to the planetary ephemeris frame and the Hipparcos optical frame, thereby creating a unified system that is much more valuable than the sum of the separate constituent frames.

---

[1] Tracking Systems and Applications Section.

[2] NASA Graduate Student Research Program Fellow, Department of Physics, University of Arizona, Tucson, Arizona.

[3] Retired from the Tracking Systems and Applications Section.

I. Historical Background

Astronomical objects have been used for millenia to construct reference frames for measuring the passage of time, for navigation, and for solar system dynamics. Early astronomers measured the motions of the planets against the background of "fixed" stars. As observations improved, systematic motions of these "fixed" stars became evident. Hipparchus is credited (e.g., [23]) with recognizing precession as early as 129 B.C. Further major advances in astrometry awaited the invention of the telescope. Proper motions were first observed by Halley in 1718 [37]. The ≈20-arcsec annual aberration due to the Earth's orbital motion was first observed by Bradley [8] in 1729. A few decades later, he also was the first to observe the ≈9-arcsec effect of the Earth's 18.6-year nutation [9]. Attempts to measure meridian transit times of stars to better than 1 s forced F. W. Bessel in 1816 to realize that differing observer reaction times were biasing results. This may be the first time in astronomy that the dependence of the observations on the observer was appreciated [19]. Parallaxes of individual stars were observed by Bessel [4] in 1838. The effects of precession, proper motion, aberration, nutation, and parallax on the positions of astronomical objects are still areas of active research in modern astrometry. While the use of modern electronics has minimized the influence of the human observer on the raw observations, we still are very much concerned with the influence of the analyst on the results of data analysis. Following the discussion of the development of extragalactic astronomy by Ma [61], we note that as observing precision continued to improve, scientists such as Herschel and Laplace suggested using extremely distant objects to define astrometric reference frames. Such objects reduce the effects of proper motion and parallax on reference frame definition. The catalogs of Messier [67], Herschel [41], and Dreyer [22] were important steps in identifying these more distant objects. The work of Leavitt [54] with Cepheid variable stars in 1912 and the work of Hubble [44] in 1925 to measure the distance to M31 (the Andromeda galaxy) helped to establish the extreme distances of what are now classified as extragalactic objects. The connection between the redshift and the extreme distance of extragalactic sources was made by Hubble [45] in 1929.

Radio frequency observations of these extragalactic objects were pioneered by Jansky [50] in 1932 and Reber [76,77] in the 1940s. The third Cambridge survey [24] and the Parkes surveys (e.g., [6]) identified many of the radio sources used today. Early in the development of very long baseline interferometry (VLBI), source positions were measured with an accuracy of from 1 to 3 arcsec [16]. Within a few years, Wade and Johnston [100] were able to achieve accuracies of ≈30 milliarcseconds (mas) using a connected-element interferometer.

During the 1970s, the Jet Propulsion Laboratory (JPL) began a VLBI program with applications in astrometry, geodesy, and spacecraft navigation. The JPL VLBI group's first published radio source positions were given in 1984 by [27], with 2- to 5-mas accuracy, and were updated in 1988 by [88] to a 1- to 2-mas level of accuracy. This article reports on the progress of the JPL program to ≈0.3-mas accuracy. Related programs have been carried out at the Goddard Space Flight Center (GSFC), the National Oceanic and Atmospheric Administration, and the U.S. Naval Observatory (e.g., [15], [80], [62], and [51]).

During the past decade, the International Earth Rotation Service (IERS) has served to coordinate the efforts of the various radio astrometric groups. The IERS has combined the results of these groups into a uniform celestial reference frame that was updated on a yearly basis through 1995 [1]. In the fall of 1995, the IAU's working group on reference frames produced the International Celestial Reference Frame (ICRF), which was used by [56] to link the Hipparcos mission's optical catalog—with its 1-mas positions and 1-mas/yr proper motions for 120,000 stars—to the extragalactic radio frame. In August 1997, the IAU formally adopted a new International Celestial Reference System [47] that replaced the Fundamental Katalog 5 (FK5) reference system effective January 1, 1998. The new system is realized at radio wavelengths by the ICRF [64] and at optical wavelengths by the Hipparcos catalog [25]. The dynamical frame of the JPL planetary ephemeris [92] also has been linked, by several techniques, to the extragalactic radio frame. With these links in place, the inherent stability and accuracy of the extragalactic celestial frame is now accessible to a much wider group of astronomers and techniques.

II. Introduction

The extragalactic radio reference frame has been used for deep-space navigation (e.g., [7]), Earth orientation measurements (e.g., [46]), geodesy (e.g., [26]), and astrometry (e.g., [88], [62], [99], [72], [48], and [51]). In addition to the intrinsic scientific interest in the stability of dynamical systems, these varied applications require accurate and stable positions of the objects composing the reference frames. Over the last two decades, several research groups have used the VLBI technique to catalog positions of extragalactic radio sources. The work on radio reference frames at JPL was begun in support of interplanetary spacecraft navigation—an interest that was unique to JPL.

The purpose of this article is to report the source coordinates that constitute the extragalactic radio reference frame; to assess the accuracy of these positions; to compare the JPL celestial frame with the new IAU fundamental frame; and to review the current status of the frame ties made between the radio, the Hipparcos optical, and the planetary ephemeris frames. The discussion is arranged as follows: Section III will briefly discuss the experimental technique, accumulated data, and analysis procedures that were used to derive the current JPL radio frame. Section IV will discuss observable modeling, weighting, and parameter estimation. Section V will present the results that comprise the frame. Section VI will discuss the accuracy of the VLBI radio reference frame on the basis of internal consistency criteria. Special attention is given in this section to "local" stability as measured by apparent proper motions of individual sources and to "global" stability as measured by estimates of precession and nutation. Section VII will discuss the accuracy of the frame inferred from comparison with independent results. Section VIII will compare the results of this article with the newly adopted ICRF in order to provide an assessment of the accuracy of this new international standard. Lastly, Section IX will review the techniques used to connect the radio, optical, and ephemeris frames and the estimated accuracy of such ties. These connections allow the radio frame to be useful to a wider range of observers.

III. Experimental Techniques

Astrometric VLBI experiments to obtain extragalactic radio source positions have been carried out by JPL since the early 1970s. This program has been motivated by the need to provide an accurate reference frame for navigating interplanetary spacecraft. The resulting catalog of radio source positions defines this radio reference frame. Our observations were made using the Deep Space Network (DSN) 34- and 70-m antennas near Goldstone, California; Madrid, Spain; and Tidbinbilla, Australia. This section reviews the experimental techniques that were used to obtain the observables from which our results were generated. The discussion will cover, in order, each step in the VLBI technique: first, the strategy used in experiment design, followed by overviews of signal collection, post-collection digital signal processing, and data editing. These steps lead to observables that then are gathered into a large data set, which is described at the end of this section.

A. Experiment Strategy

Good VLBI experimental technique begins with the design of an observing strategy from which one may create a strong schedule of sources to be observed. To that end, data typically were collected in sessions lasting 24 hours. Sessions of this length allow the full range of right ascensions to be observed. Furthermore, day-long sessions are important so that diurnal effects such as nutations can be well measured. Occasionally, instrumental problems or scheduling conflicts with spacecraft tracking reduced antenna availability, forcing the session to be shorter than the desired 24 hours. Typically, observing sessions involved two stations. While a larger network would have provided a stronger observing geometry, the limited availability of an expensive resource prevented inclusion of more stations. In order to create a strong geometry and minimize the effects of systematic errors, sessions were designed with a goal of observing 80 to 100 distinct sources, each at two or three different hour angles. A typical observation lasted $\approx$2 minutes. Our observing schedules attempted to balance a desire to maximize the number of sources observed against the need to sample the full range of mutual visibility more quickly than delay model parameters change (e.g., troposphere). The first goal argues for short antenna slews between

nearby sources, whereas the second goal argues for long, time-consuming slews between widely separated sources. In practice, a compromise was made between these conflicting goals: the schedule stepped through sources that are nearby in declination so that the antenna cycled from high to low and back to high declination in about 2 hours. This procedure allowed a relatively quick variation of the antenna elevation angle in order to separate troposphere and station vertical parameters while keeping the slew distance between sources relatively small. This strategy contributed to positive correlations between declination estimates that typically are 15 to 20 percent. Furthermore, on the very long California–Australia baseline, the source right ascension is highly correlated with time (and, thus, the clock parameters) due to the narrow range of hour angles that provides mutual visibility from both stations. Distinct observing schedules were designed for each session, in part to accommodate the gradual infusion of new sources. In the mid-1980s, the observing program included slightly over 100 sources. It now encompasses nearly 300 sources, including many near the ecliptic plane, for possible use in spacecraft navigation, as well as about a dozen sources that were needed for the frame tie between the radio frame and the Hipparcos optical frame.

B. Signal Collection

Given an experiment design, we now proceed to the process of collecting the signals from the sources of interest. In this process, widely separated antennas, large apertures, highly stable frequency standards, low system temperatures, and large spanned bandwidths all contribute to measurement quality. Depending on availability, we used one of four Deep Space Station (DSS) antennas (DSS 12, DSS 13, DSS 14, or DSS 15) at the Goldstone, California, antenna complex and one of three at the Australia (DSS 42, DSS 43, or DSS 45) and Spain (DSS 61, DSS 63, or DSS 65) complexes. The approximate lengths of the two available baselines are 8,400 km for California–Spain and 10,600 km for California–Australia. The 12,000-km Spain–Australia baseline is nearly an Earth diameter in length and, therefore, does not provide a wide enough range of mutually visible sources to be useful for VLBI measurements. All of our experiments used H_2 maser frequency standards. Nearly all the data acquired since mid-1989 used the DSN's 34-m high efficiency antennas (DSS 15, DSS 45, and DSS 65). The receiving systems of these 34-m antennas typically had a system temperature of 35 K at zenith, increasing by 2 to 4 K per air mass for observations away from zenith. In addition, the 34-m antennas were equipped with cryogenically cooled low noise transistor amplifiers having 100-MHz spanned bandwidths at S-band (2200 to 2300 MHz) and nearly 400-MHz bandwidths at X-band (8200 to 8600 MHz). These radio frequency bands were heterodyned down to intermediate frequency (IF) bands of 200 to 300 MHz for S-band and 100 to 500 MHz for X-band. The IF signals were sent via coaxial cables from the antenna to a signal-processing building where a second stage of heterodyning produced a nonoverlapping set of baseband (0- to 2-MHz) channels that included five S-band channels and nine X-band channels for most experiments. Because the local oscillators used in the second stage of heterodyning had degraded phase stability at the 100- and 500-MHz extremes of their nominal operating range, data were taken only in the range of 116 to 483 MHz in order to minimize phase errors. A detailed explanation of the placement of the baseband channels is given by [34]. After the signal was divided into baseband channels, each baseband channel was 1-bit sampled at a rate of 4 Mbits/s and then recorded on digital video tape for later processing. The 2-MHz baseband channels actually are seven-pole Butterworth filters with a -3 dB point at 1.8 MHz. Thus, the 4-Mbits/s sample rate slightly oversamples the data, causing small correlations of $\approx$10 percent. The processing ignores these correlations. The sample rate was chosen so as to balance degradation from oversampling (correlated data) against aliasing—which would fold unwanted signals back into the sampled data. For each source observation, the signal was integrated for $\approx$2 minutes in order to build up the signal-to-noise ratio (SNR). In summary, the long baselines, large antenna apertures, highly stable frequency standards, low system temperatures, and large spanned bandwidths of the DSN combine to form an extremely powerful astrometric instrument. The long baselines provide very high angular resolution; the large apertures and low system temperatures yield very sensitive detections; and the stable frequency standards enable long coherent integrations that further enhance sensitivity. The large spanned bandwidths provide a long lever arm for determining group delays from the variation of phase as a function of frequency.

C. Signal Processing

For each antenna in a VLBI experiment, the incoming microwave signal from an extragalactic radio source was amplified, downconverted and filtered into several 2-MHz-wide subchannels, 1-bit sampled, and recorded on magnetic tape. The tapes then were brought to a custom-designed signal-processing center known as the correlator, where the digitized voltages, $V_n(t)$, as a function of time, t, were read in from each of two stations $n = 1, 2$. Next, the two voltages were offset in time ("delayed"), multiplied together, and integrated over a period of time, T, to form the cross-correlation coefficient, ρ,

$$\rho(\tau) = \frac{1}{T}\int_0^T dt V_1(t) V_2^*(t-\tau) \tag{1}$$

where τ is the time offset or delay between the two streams of sampled voltages and $*$ indicates the complex conjugate. In order to emphasize only the most important concepts, various normalization factors are ignored in the expression for ρ. The correlation coefficients were determined for a set of 14 frequency channels and a series of 2-second time integrations for each radio source. The phases, $\phi(\omega_i, t_j)$, of these correlation coefficients as a function of the frequency channels, ω_i, and the integration times, t_j, were then least-squares fit to a bilinear function:

$$\phi(\omega_i, t_j) = \phi_0 + \frac{\partial\phi}{\partial\omega}(\omega - \omega_0) + \frac{\partial\phi}{\partial t}(t - t_0) \tag{2}$$

where the estimated phase slope versus frequency is the group delay,

$$\tau = \frac{\partial\phi}{\partial\omega} \tag{3}$$

and the estimated phase slope versus time is the phase delay rate,

$$\dot{\tau} = \frac{\partial\phi}{\partial t} \tag{4}$$

These are the two observables used in astrometric VLBI. Because tropospheric turbulence degrades the phase delay rates, most of the astrometric and geodetic information is contained in the group delays, which may be crudely modeled as follows:

$$\tau = \tau_{geom} + \tau_{clock} + \tau_{trop} + \tau_{tide} + \tau_{\epsilon} \tag{5}$$

The term τ_{geom} accounts for the geometric separation of the antennas and may be many milliseconds for Earth-based baselines. The term τ_{clock} accounts for the lack of synchronization of the frequency standards, or clocks, and is $\approx$1 μs. The term τ_{trop} accounts for the additional signal delay due to the troposphere (compared with the signal in a vacuum) and typically is tens of nanoseconds. The term τ_{tide} accounts for various tidal effects that may amount to a nanosecond. Numerous small effects (e.g., plasma effects, source structure, and antenna thermal expansion) are collected into the term τ_{ϵ}. The geometric delay clearly is the largest term by several orders of magnitude and deserves a more detailed explanation. It is determined from the scalar product of the vector baseline between two stations, $\mathbf{B}$, and the unit vector in the source direction, $\hat{\mathbf{s}}$, normalized by the speed of light, c:

$$\tau_{geom} = \frac{\mathbf{B}\cdot\hat{\mathbf{s}}}{c} \tag{6}$$

The accurate determination of the source direction vector, $\hat{\mathbf{s}}$, is the principal subject of this article.

D. Data Editing

At various stages of the signal processing, one must remove or "edit" corrupted data. In an ideal system, all scheduled observations would be used in determining parameters of physical interest. However, inevitably there are problems that occur in data collection and processing that corrupt some of the data. Procedures have been developed that attempt to excise the corrupted data on the basis of objective criteria so as to avoid eliminating valid data. There always is a temptation to eliminate data that are not well explained by existing models in order to "improve" the agreement of theory and experiment. Such an approach may, of course, eliminate the very data that would indicate deficiencies in the a priori model and thereby preclude the discovery of improved models. Thus, the need arises for objective editing criteria. The first editing steps focus on eliminating data that were degraded due to imperfections in the recording process. The recordings were done on 1-inch-wide video tapes at a data rate of 56 Mbits/s. The recording process augments the data stream with 1 parity bit for every 8 bits of data, and once every 5 ms a "frame header block" is recorded to assist in tape synchronization. At tape playback time, data with bad parity were eliminated from the data stream. Typical parity error rates were less than 10^{-3}. Data with bad frame header blocks were retained at tape playback due to hardware limitations but later were eliminated in software if the frame error rate was greater than 1/s (0.5 percent). If instrumental phase stability in any channel—as measured by instrumental phase calibration signals [87]—was worse than 5 deg root-mean-square over a source observation (typically 2.5 minutes), the data usually were eliminated. Exceptions were made in cases where the calibrations were unstable because they were measuring and correcting known problems in instrumentation. In the processing stage that fit the phase samples, checks were made to ensure that there were no integer cycle slips in the data stream that could corrupt the phase rate. Cases where this procedure detected the need for cycle corrections were flagged in the database and often individually examined by an analyst. This procedure was limited to measurements for which the SNR was sufficiently high to divide an observation into several smaller integrations. The phase-fitting software estimated a "detection" SNR based on maximum signal amplitude divided by an empirical measure of amplitude noise for the whole frequency band (typically composed of five to nine channels). This measure was interpreted as follows:

0–5 nondetection :	data eliminated to avoid a high probability of false detection
5–10 marginal detection :	data examined by analyst
10–30 good detection :	data accepted
>30 strong detection :	able to check phase variations within an observation

If the SNR in any given channel was less than 1/4 of the mean SNR for the whole band, the problematic channel was eliminated. Unfortunately, these procedures were not followed uniformly because software development was an ongoing effort. Where possible, data were reprocessed. Most data taken since 1989 were checked with most of the above criteria. Finally, the modeling and parameter estimation software determined residuals relative to our best models. If residuals were greater than five times the modeled uncertainty (as described in Section IV.B), the data points were labeled outliers and eliminated from the final parameter estimation. Data taken before $\approx$1989 were not as carefully and objectively checked in the early stages of processing and, therefore, relied more heavily on this outlier test to identify and remove degraded data. Finally, we note that data eliminated from the final solution by the outlier test are still retained in the data archives for possible reinclusion as future modeling improvements may allow.

E. Data Set

Having briefly reviewed experiment design, observable generation, and data editing procedures as used in astrometric VLBI, we now describe the set of observables that will serve as the basis of this article. In addition, references are given that describe in detail the algorithms used to process these

observables. The data set consists of 26,546 observable pairs of delay and delay rate covering a time span from October 1978 to April 1996. These data were acquired using the MkII system[4] [68,14] from 1978 to 1989 when 8,615 observations were collected, and subsequently using the MkIII system [84] from 1988 to 1996 when 17,931 observations were collected. For some later MkII data and almost all MkIII data, the instrumentation was phase calibrated [83,94] in real time using the system designed by Sigman [87]. From 1978 to 1987, the MkII data were correlated at the JPL/Caltech Block0 correlator [95] and after 1987 at the JPL BlockII correlator [96].[5] All the MkIII data were correlated at the JPL BlockII correlator. Post-correlation signal processing of the Block0 correlation results was done with the PHASOR software.[6] BlockII correlator output was processed with the FIT software [59]. The FIT software determines group delays using the bandwidth synthesis technique [82]. This technique uses several narrow channels to span a wide radio frequency band with just a fraction of the recording bandwidth that would be required if the entire band were sampled (a "filled" band). In the majority of our experiments, five channels of 2-MHz width were spread over the S-band range from 2200 to 2300 MHz and nine channels of 2-MHz width were spread over the X-band range from 8216 to 8583 MHz (cf., [34] for details of the design of our channel spacings). Thus, the group delays—which measure the phase change versus frequency—benefit from a large 367-MHz lever arm for measuring the phase versus frequency slope while requiring the recording system to sample less than 5 percent (18 MHz of the 367 MHz) of the total X-band range. The FIT software used the simultaneously recorded S-band and X-band signals to calibrate the charged-particle effects of the Earth's ionosphere, solar plasma, and interstellar plasmas. Instrumental effects were calibrated for a few of the later MkII experiments and the great majority of the MkIII experiments with the phase calibration system designed by Sigman [87]. The FIT software applied both the correction for charged-particle effects and the instrumental phase calibrations. The theoretical modeling of the group delays and phase delay rates was done with the MODEST software [90]. Surface pressures and temperatures from each site were used to partially calibrate tropospheric effects at this stage of the processing. After applying the a priori theoretical model, the MODEST software estimated linearized least-squares adjustments to the model parameters using a square root information filter (e.g., [5]).

IV. Observable Modeling, Weighting, and Parameter Estimation

Once observables are produced using the techniques described in the previous section, the next step is to compare the results to the theoretical predictions of "standard" models. After the differences between theory and experiment have been obtained, their significance must be assessed on the basis of calculations of the expected measurement errors. These expected errors then are used to weight a least-squares adjustment to parameters that describe the theoretical model. This section will briefly describe these three steps of the analysis: theoretical modeling, data weighting, and parameter adjustment.

A. Observable Modeling

Modeling of the group delays and phase delay rate observables is described in detail in [90,91]. We will present here a brief summary. In general, modeling of the VLBI observables is consistent with the IERS conventions [66]. We use the tropospheric mapping function of Lanyi [53] with its input parameters taken from the temperature versus altitude profiles given in the 1965 U.S. Standard Atmospheres [18]. The use of the U.S. Standard Atmospheres follows the approach of Niell [71].

Of particular importance to the establishment of a celestial reference frame are those portions of the model that determine the overall orientation of the frame. First, note from Eqs. (5) and (6) that the principal VLBI observable, the group delay, measures primarily the scalar product of the baseline

[4] E. J. Cohen, *VLBI Bandwidth Synthesis Manual*, (internal document), Jet Propulsion Laboratory, Pasadena, California, June 1979.

[5] T. O'Connor, *Introduction to BlockII VLBI Correlator Hardware*, (internal document), Jet Propulsion Laboratory, Pasadena, California, April 1, 1989.

[6] G. H. Purcell, Jr., personal communication, Jet Propulsion Laboratory, Pasadena, California, 1983.

vector, **B**, and the source position vector, $\hat{\mathbf{s}}$: $\tau = \mathbf{B} \cdot \hat{\mathbf{s}}/c + \tau_{clock} + \tau_{atmo} + \tau_{tide} + \tau_{\epsilon}$, because the clock, atmospheric, tidal, and other small effects, represented by the four rightmost terms, almost always are several orders of magnitude smaller than the geometric delay represented by the first term on the right. Since the scalar product $\mathbf{B} \cdot \hat{\mathbf{s}}$ is rotationally invariant, VLBI measures—to a very good approximation—the *relative* orientation of the baseline and the source vector. Thus, the set of source positions that later will be presented as the chief result of this article are *almost* indistinguishable from a set that has been rigidly rotated from the original set. However, this rotational freedom is not completely unconstrained due to three factors: first, the sensitivity of the τ_{atmo} term to the elevation of the source above the horizon; second, the sensitivity of the τ_{tide} term (as well as gravitational retardation) to the direction of the Sun, Moon, and planets; and third, the sensitivity of the τ_{geom} term to the velocity vector required to Lorentz transform (aberrate) **B** and **s** into a common frame of reference. While a complete analysis of these sensitivities is beyond the scope of this article, a simple numerical analysis was done to quantify the constraints that the aforementioned effects place on the rotational freedom of VLBI measured source positions. This analysis removed the standard constraint on the origin of right ascension (RA). In the resulting catalog of source positions, the median RA formal uncertainty increased by more than a factor of 1000 to 182 mas. However, it is important to note that the RA parameters also became nearly perfectly correlated. As a result, a comparison of the actual coordinate shifts induced by the lack of an RA constraint shows only a factor of 10 degradation (several mas) as long as all correlations are accounted for. Thus, with the present sensitivity of VLBI, the set of source positions is rotationally constrained at the few-hundred-mas level by the data themselves.

In order to avoid the extreme correlation of RA parameters and the mas-level degradation of the source positions, the rotational freedom of the estimated source right ascensions was constrained by assigning a conventional origin of RA (α_0) rather than relying on the direct measurement sensitivity. The RA of the source GC 0235+16 (α_0 = 2 hr 38 min 38.9301040 s) was adopted as the conventional origin in agreement with the new ICRF [64]. Given the origin α_0, the orientation of the baseline relative to this frame must be specified. The a priori Earth orientation (UT1–UTC and polar motion) positions the baseline relative to the Earth's pole based on the SPACE96 series of [35] augmented by the diurnal and semi-diurnal ocean tidal UT1–UTC and polar motion model of [89]. The retrograde diurnal portion of this short-period ocean model is indistinguishable from nutation and, therefore, contributes to the frame's orientation. The pole then is oriented relative to the celestial frame using the IAU 1977 model of precession [57] corrected by −3.0 mas/yr, and the Zhu–Mathews Oceans Anelasticity (ZMOA) 1990–2 model of nutation [39] instead of the less accurate IAU 1980 standard nutation model [101,86]. For the reference day of March 14, 1992, this model also is augmented by offsets in ecliptic longitude of $\Delta\psi_0 = -42.161$ mas and obliquity of $\Delta\varepsilon_0 = -5.817$ mas, which constrain our frame to be aligned with the ICRF. For days other than the reference day, we estimate offsets in $\Delta\psi$ and $\Delta\varepsilon$ to account for remaining deficiencies (see Fig. 1) in the a priori precession–nutation model described above. To summarize, our frame's orientation has been aligned with the ICRF by augmenting the a priori models of UT1–UTC, polar motion, precession, and nutation with three constants: α_0, and $\Delta\psi_0$ and $\Delta\varepsilon_0$—the celestial pole offset on March 14, 1992. Having discussed observable modeling, we now turn to the weighting of the data.

B. Data Weighting

Considerable effort has gone into accurately estimating the measurement errors in the observables. These errors provide the data weights necessary to accurately estimate the parameter adjustments (e.g., source positions) and their associated uncertainties. To the extent that measurement errors are accurately modeled, the parameters extracted from the data will be unbiased and will have accurate covariances assigned to them. While some unidentified and unmodeled errors remain, we believe that the largest ones have been identified: mismodeling of troposphere azimuthal asymmetry (Section VI.A.9) and the troposphere temperature profile (Section VI.A.8). These two systematic errors have not been accounted for in the a priori measurement errors, and, consequently, they are not accounted for in the data weights. These two errors will be treated in the aforementioned sections. These systematic errors aside, the largest

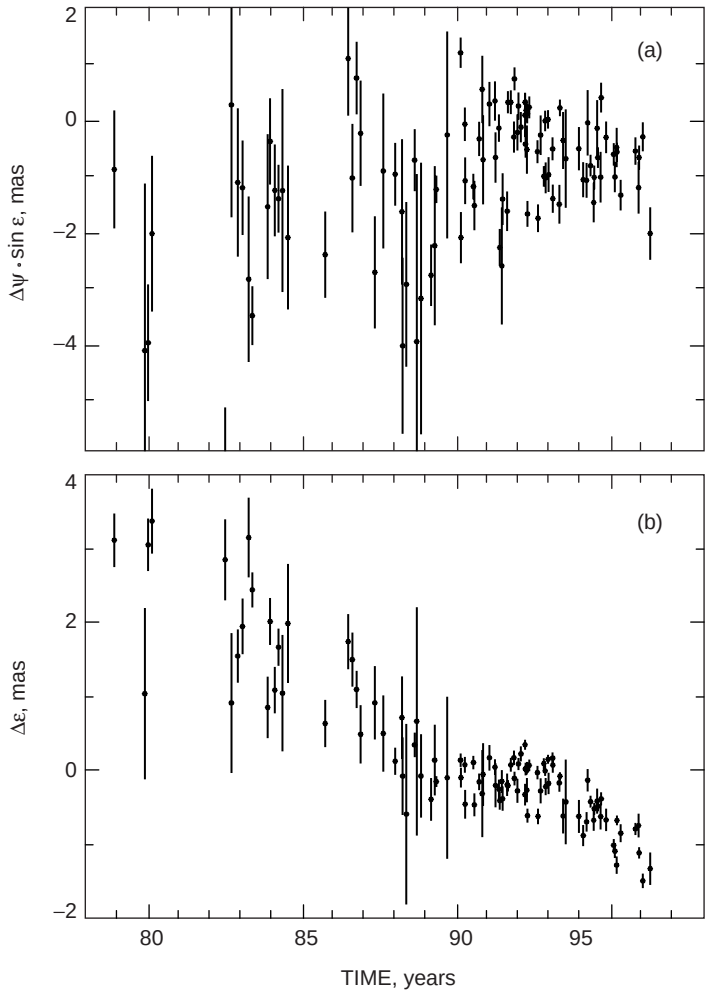

Fig. 1. Offsets of the celestial ephemeris pole from the a priori model in Section IV.A: (a) ecliptic longitude and (b) obliquity. If a model composed of a linear term plus harmonic terms at 18.6-, 9-, 1-, and 0.5-year periods is removed from the data points, the wrms residuals are 277 and 228 μas in $\Delta\psi$ sin ε and $\Delta\varepsilon$, respectively. Note the improvement in data quality c.1989 when the introduction of the MkIII recording system increased the recorded bit rate from 4 to 56 Mbits/s and the spanned bandwidth from 40 to 367 MHz.

source of stochastic error is refractivity fluctuations caused by turbulence in the water vapor layer in the lower troposphere. The next two largest errors arise from instrumentation and source structure. We now will examine these three known sources of error in turn.

1. Troposphere. The largest source of error that has been modeled is random fluctuations in the water vapor distribution in the lower troposphere. For reasons that will be presented below, the data were analyzed using a Kolmogorov model of the spatial and temporal fluctuations in refractivity caused by tropospheric turbulence. This model requires that the analysis treat the observations as being correlated.

With that in mind, we first will examine the residuals (observed − model) of an analysis that assumes uncorrelated errors in the troposphere model. This simplified analysis provides evidence for the considerable impact of the tropospheric delay on VLBI observations. Figure 2 shows the increase in weighted root-mean-squared (wrms) residual phase delay rates and group delays as the path length through the

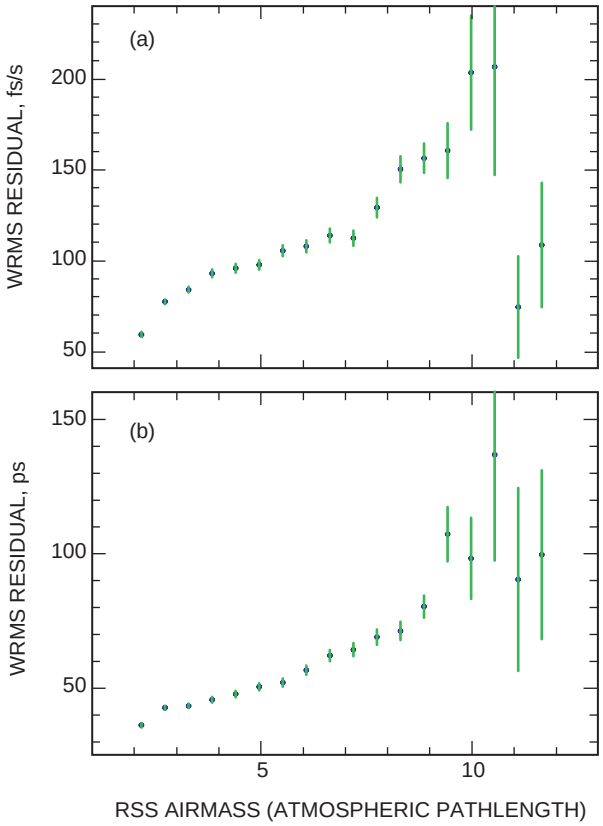

Fig. 2. The wrms residual (a) phase delay rate and (b) group delay versus rss tropospheric path length of the observation's ray path. Path lengths are normalized to the zenith path at one station. Error bars are proportional to the square root of the number of observations in each bin in order to indicate the relative weight of each bin.

atmosphere increases. If station i is observing at elevation angle E_i, above the horizon, the troposphere thickness normalized to the zenith thickness is $\approx \mathrm{csc E_i}$ air masses. Assuming that the tropospheric modeling error at each station is proportional to the atmospheric path length and that the errors are independent for widely separated stations, the total delay error then would be expected to be proportional to the root-sum-square (rss) of the path lengths ($\propto \sqrt{\mathrm{csc^2 E_1 + csc^2 E_2}}$). Figure 2 shows that these assumptions are borne out in the data. If the modeled errors do not include terms to account for tropospheric fluctuations, χ^2_ν's (where ν is the number of degrees of freedom that have been used to normalize χ^2) corresponding to the residuals shown in Fig. 2 also increase as the rss air mass increases. This indicates that the increase in residuals is not fully accounted for by the reduced instrumental sensitivity (i.e., the 2- to 4-K per air mass increase in system temperature) at high air masses. Independent evidence from water vapor radiometry that VLBI residuals are dominated by wet tropospheric refractivity fluctuations is presented in [93]. Note that unmodeled azimuthal gradients (e.g., [32]) in the troposphere are expected to cause errors proportional to $\approx \mathrm{csc}^2 E_i$ (at low elevations), and errors in modeling the profile of the temperature as a function of altitude are expected to cause errors proportional to $\approx \mathrm{csc}^3 E_i$. Therefore, the absence of a clear quadratic or cubic signature in Fig. 2 may be interpreted as evidence either that these types of errors are not dominant or that they are efficiently absorbed by nontropospheric parameters (e.g., station locations, nutations, etc.). In fact, the evidence to be presented in Section VI.A.9 will suggest that azimuthal gradients may be efficiently absorbed by shifting the source positions smoothly over a broad zone as a function of declination.

Tropospheric turbulence is perhaps the most difficult error source to model adequately. We use the Treuhaft and Lanyi model [98] (hereafter referred to as T-L) for the observation covariance due to tropospheric turbulence. Briefly, they model the troposphere noise as Kolmogorov turbulence in the water vapor spatial distribution near the surface (up to 1 to 2 km). They further assume that temporal correlations may be modeled by a constant wind (≈10 m/s) carrying a fixed spatial distribution over the antenna. As ray paths become separated by more than the 1- to 2-km scale height, the three-dimensional turbulence becomes two-dimensional. This model accounts for both spatial and temporal correlations between observations. In contrast, stochastic filtering techniques (e.g., [40,97]) account only for the temporal correlations. Assuming that the delay rate scatter is dominated by troposphere noise, we use this scatter to estimate the turbulence magnitude (C_n in the notation of T-L) for each baseline during each experiment. Finally, the ratio of wet zenith troposphere delays is used to constrain the ratio of C_n's at the two stations of a given baseline. In this sense, our covariance model is self-calibrating. In the interest of keeping the computational complexity at a manageable level, two simplifications were made. First, troposphere covariance between sessions (time spans of a few days to a few months) was assumed to be zero. Second, the correlations between phase delay rate observations always were assumed to be zero on the basis of a study by Linfield,[7] which concluded that the correlations typically start at ≤10 percent and decay to smaller values on time scales of a few minutes. The T-L observation covariance significantly improves the wrms repeatability of the daily estimates of baseline length as compared with a simpler diagonal covariance model (i.e., one that ignores correlations between observations). After removal of a linear trend to account for tectonic motion, the wrms baseline length scatter is 31 mm for the California–Australia baseline and 16 mm for California–Spain using a simple (uncorrelated) observation covariance to account for troposphere noise. Application of the T-L covariance model improves these repeatabilities to 24 and 13 mm on the two respective baselines—improvements of 20 and 9 mm in quadrature, respectively. For this reason, we chose to use the T-L troposphere covariance model rather than mathematically simpler alternatives.

While the model described above accounts for an important type of troposphere error, there are other types of potential error that have not been modeled in the observation covariances. These include errors in the temperature-versus-altitude profile of the troposphere and persistent azimuthal asymmetry (gradients) in the troposphere [32,65,13]. The discussions in Sections VI.A.8 and VI.A.9 will attempt to establish bounds for these errors.

2. Instrumentation. The thermal noise from the receiving electronics has been modeled as white noise. Observations collected with the MkII system (1978–1989) have median uncertainties due to thermal noise of 204 ps for group delays and 10 fs/s for phase delay rates. Observations made with the MkIII system (1988–1996) had much lower thermal noise due to order-of-magnitude increases in the recorded data rate and the total spanned bandwidth. Details of the thermal noise calculation for MkIII data are given in [59]. For the MkIII data, the median uncertainties due to thermal noise were 10.7 ps for group delays and 4.9 fs/s for phase rates. The distribution of measurement uncertainty due to the MkIII system's thermal noise is shown in Fig. 3. As can be seen from comparison with the size of the troposphere noise shown in Fig. 2, the thermal noise is not a dominant error source for MkIII data.

An additional 25 ps of white noise was added in quadrature to account for any uncalibrated delay changes in the chain of receiving electronics and drifts in the H_2 maser atomic clocks. Because the delay rates are dominated by troposphere noise, only 1 fs/s of noise was added in quadrature to the rates. We currently are examining ways to model the correlated delay errors from atomic clock wander. Preliminary studies indicate that this error source may affect estimated source positions by as much as 75 μas.

[7] R. P. Linfield, "Troposphere Delay Rate Statistics for VLBI," JPL Interoffice Memorandum 335.1-95-023 (internal document), Jet Propulsion Laboratory, Pasadena, California, August 1995.

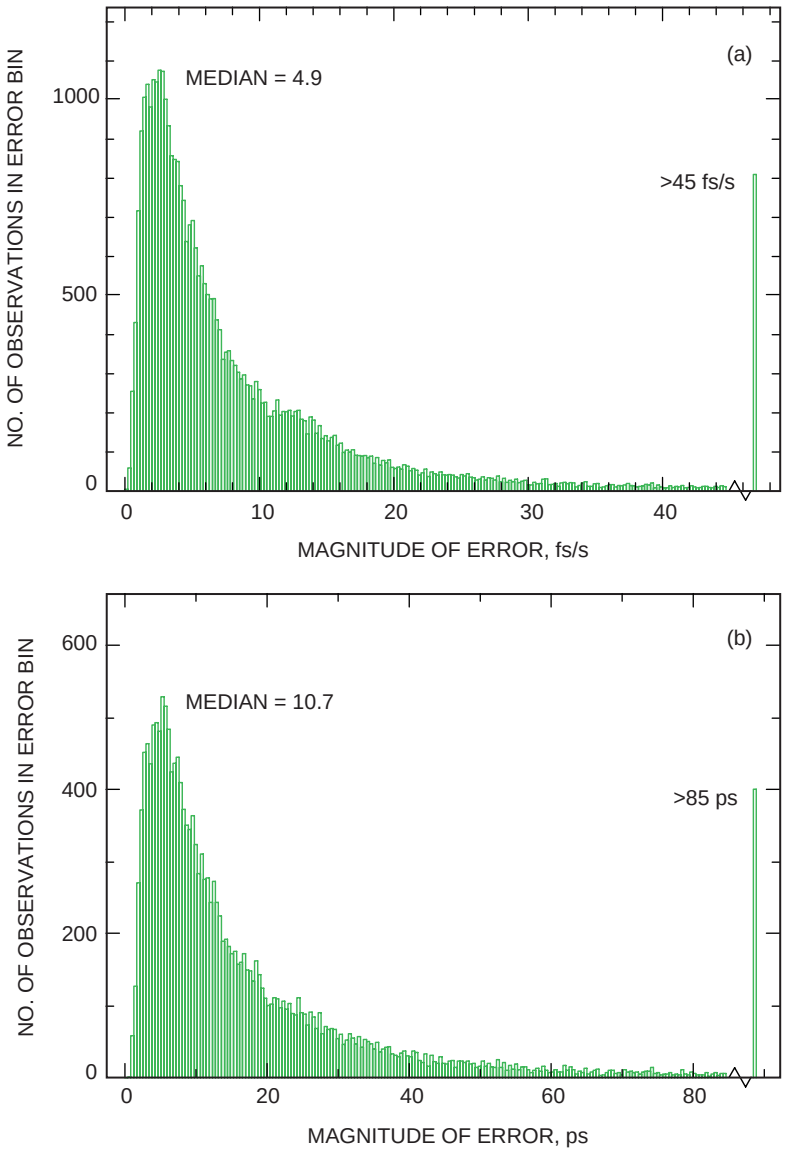

Fig. 3. The distribution of the modeled measurement uncertainty due to thermal noise from the receiving electronics for the 17,931 observations made with the MkIII system (1988–1996): (a) the phase delay rate and (b) the group delay. Points with uncertainties in excess of 45 fs/s or 85 ps are merged into the rightmost bins.

3. Source Structure. The third error source that has been modeled a priori in our analysis accounts for the spatially extended nature of the radio sources. Most sources observed at radio frequencies are now known not to be point sources at the submilliarcsecond level (e.g., [29,28]), which is of interest to the present discussion. Charlot [11] has demonstrated that source structure can be modeled successfully in a study of one source: 3C 273. However, the time- and frequency-dependent brightness distribution maps that are necessary to correct for non-point-like source structure currently are available for only a fraction of our observations. Thus, lacking adequate models, we must treat source structure as a measurement error. For about 10 percent of the sources, this error is a significant error source. For these sources, we have added source-specific white noise to the observation uncertainty in order to make $\chi^2_\nu = 1$. Table 1 shows this additive group delay noise, which ranged from 30 to 180 ps over a set of 36 non-point-like sources. Similarly, Table 2 shows the additive delay rate noise, which ranged from 50 to 100 fs/s for

Table 1. Delay additive noise due to source structure.

Noise, ps	Source
30	0212+735
	P 0332−403
	P 0420−01
	P 0646−306
	P 1510−08
	B2 2201+31A
	CTA 102
	3C 454.3
60	0016+731
	0440+345
	P 0743−006
	3C 279
	P 1435−218
	P 1504−167
	P 1511−100
	P 1622−253
	GC 1633+38
	P 1821+10
	3C 390.3
	3C 395
	1928+738
	OX 036
	P 2128−12
	P 2345−16
90	3C 120
	P 1127−14
	OT 465
	OW 637
120	3C 84
	0919−260
	3C 273
	1826+796
	P 2127+04
150	P 0237−23
	1947+079
180	OI 417

a nonoverlapping group of 19 sources. It is peculiar that there are no sources in common to both tables; the reason for this is unknown to us. Note that many of the sources in these tables are referred to by more than one name. Standard names based on B1950 positions are given in Table 5. A more complete dictionary of aliases can be found in [63] or at http://hpiers.obspm.fr/webiers/results/icrf/dico.html. While this noise model is rather crude, it has the virtue of producing more realistic estimates for the source position errors and of downweighting "bad" sources so that they do not corrupt the fit for "good" sources.

To verify the effectiveness of this noise model, two tests were done. In the first test, the standard solution was modified by removing the source structure portion of the noise model. This change worsened the repeatability of the baseline length for both baselines. For source positions, changes were judged by comparing the two JPL solutions to the GSFC-1069 reference frame.[8] Agreement was measured using

[8] C. Ma, personal communication of Extragalactic Radio Source Catalog G-1069, Goddard Space Flight Center, Greenbelt, Maryland, April 8, 1997.

Table 2. Delay rate additive noise due to source structure.

Noise, fs/s	Source
50	0014+813
	P 0106+01
	DA 55
	0341+158
	OE 400
	P 0507+17
	0556+238
	0611+131
	P 0736+01
	DW 0742+10
	OJ 425
	3C 245
	GC 1342+662
	P 1349−439
	P 2254+024
	P 2344+09
100	B2 0827+24
	P 0925−203
	OW 551

the reduced χ^2 after removing a best-fit rotational difference between catalogs. Note that all sources with non-zero added source noise were excluded from the comparison in order to prevent the larger errors of these sources from decreasing χ^2 directly. Removing the added source noise from the solution worsened the goodness of the fit from $\chi^2_\nu = 5.72$ to $\chi^2_\nu = 5.80$ (for 473 degrees of freedom). In the second test, all sources with more than 100 ps of noise in Table 1 were removed from the data fed into the solution; this change altered source position scatter by $<$10 μas and created average offsets of $\leq$5 μas. The goodness of the fit (χ^2_ν) for the two baselines improved by a slight amount of $\leq$2 percent. Celestial pole position estimates did not change noticeably.

These two tests show that setting the source structure noise to zero worsens the internal consistency of the solution, whereas an arbitrarily large noise (complete downweighting of data) improves the solution by just a small amount. Thus, the structure noise model is able to desensitize the solution to the worst cases of source structure without completely eliminating the problem sources from the reference frame.

C. Parameter Estimation Strategy

Our parameter estimation strategy has been to solve for the right ascension, α, and declination, δ, of all sources except α(GC 0235+16), which is held fixed in order to provide the origin of right ascension. For each experiment (typically 24 hours of data and 200 to 300 observations), we estimate one baseline vector and corrections to the celestial ephemeris pole (offsets in ecliptic longitude and obliquity) relative to the pole model described in Section IV.A. Piecewise linear clock parameters are estimated once every 2 to 24 hours (as required by the data), and a new zenith troposphere delay parameter every 12 hours. Tropospheric fluctuations on shorter time scales are accounted for in the Treuhaft–Lanyi observation covariance model.

V. Results

The experiments considered in this article successfully observed 291 distinct compact extragalactic radio sources. Of these, 179 have been identified as quasi-stellar objects (QSOs or quasars) while 40 have

been identified as BL Lacertae-like objects (BL Lacs), 12 as Seyfert galaxies, 9 as radio galaxies [63], and the remaining 51 radio sources lack identified optical counterparts. Observations were attempted but failed for the 25 additional sources listed in Table 3. All of the observed sources are active galactic nuclei (AGNs), and their luminosity is thought to be produced by accretion onto a supermassive black hole located near the dynamical center of the host galaxy [78]. Thus, excepting sources with large-scale bright jets (e.g., 3C 273), much of the radio luminosity from AGNs is thought to come from a small but dynamically stable region on the order of 1 light year in size. Many of the sources, particularly the BL Lacs, have highly time-variable luminosities, but the *location* of the emission usually is constant. In particular, although most QSOs are compact at optical wavelengths ("star-like"), some (e.g., 3C 273) have extended, evolving radio lobes that cause their radio luminosity centroid to be time dependent and, thus, they are poor candidates for a radio reference frame unless a map of a given source is known for each epoch of observation. Nonetheless, the apparent "motion" of most quasars is not significant (see Section VI.C) for the JPL 1997-3 sources, which have a median redshift of $z = 0.97$ and range from $z = 0.004$ to 3.39.

Table 3. Sources with no successful observations.

Source	Attempted observations	Galactic latitude, deg	Ecliptic latitude, deg
0241+622	23	2.8	43.8
NRAO 150	5	−1.1	29.7
0434+299	18	−10.6	7.9
OG 050	7	−13.1	−15.7
0629+104	9	1.1	−12.8
1709−342	1	2.2	−11.3
1710−269	2	6.4	−4.0
1710−323	3	3.2	−9.4
1714−336	1	1.8	−10.6
1741−312	1	−1.6	−7.9
1748−253	2	0.0	−2.0
1817−254	1	−5.7	−2.1
1829−106	4	−1.2	12.6
1951+355	17	3.9	55.0
1955+335	22	2.1	52.8
2005+403	4	4.1	58.5
0411+054	16	−30.4	−15.4
OB 338	1	−27.2	29.4
OB 343	7	−27.5	28.9
P 0539−057	1	−17.6	−29.1
3C 48	22	−28.3	21.4
3C 286	6	80.3	36.8
P 1352−104	2	49.2	1.0
CTD 93	2	45.7	46.6
2314+03	1	−51.4	8.1

If one may assume that the large redshifts are cosmological, then the large distances and consequent small proper motions, high intrinsic luminosities, and compact nature of these objects make them ideal for determining a navigational reference frame. However, the median optical magnitude is only $V = 18.1$ (the range is $V = 12.9$ to 23.2), making the maintenance of an extragalactic reference frame extremely difficult at optical wavelengths at present. At S-band (13-cm) and X-band (3.5-cm) radio wavelengths, on the DSN baselines, the average correlated flux density is ≈0.6 Jy, while the total flux density is about 5 times higher. Detailed flux density results for the MkIII data analyzed in this article are given in [17]. VLBI using a 56-Mbits/s data rate and a pair of 34-m DSN antennas with 35-K zenith system temperatures is able to detect sources above a threshold of ≈20 mJy (5σ). Thus, these AGNs provide a spatially and temporally stable set of radio sources that is feasible to monitor for the purpose of constructing a reference frame.

Using the observations, modeling, observation weighting, and parameter estimation strategy described above (Sections III and IV), we have determined a catalog of source positions that realize the JPL 1997-3 extragalactic radio reference frame. This catalog contains right ascension and declination estimates for 291 sources. As shown in Fig. 4, these sources are fairly uniformly distributed over the sky from a declination of +85 deg down to −45 deg. Because of our need to provide sources for interplanetary navigation, we have preferentially observed in the region within 10 deg of the ecliptic plane. The denser coverage near the ecliptic plane can be seen in Fig. 4 (indicated with a dashed light blue line in the figure). In contrast, the region near the galactic plane—indicated by the orange-yellow dashed line in Fig. 4—has sparser coverage due to the difficulty of observing there. This reduced coverage is due to two problems: the lack of surveys for extragalactic sources near the galactic plane and scintillations caused by the interstellar medium. Table 3 lists sources for which repeated attempts have failed to obtain any successful observations. The first part of this table lists sources near the galactic plane (within about 10 deg); these may have gone undetected because of the scintillation problem just mentioned. This is

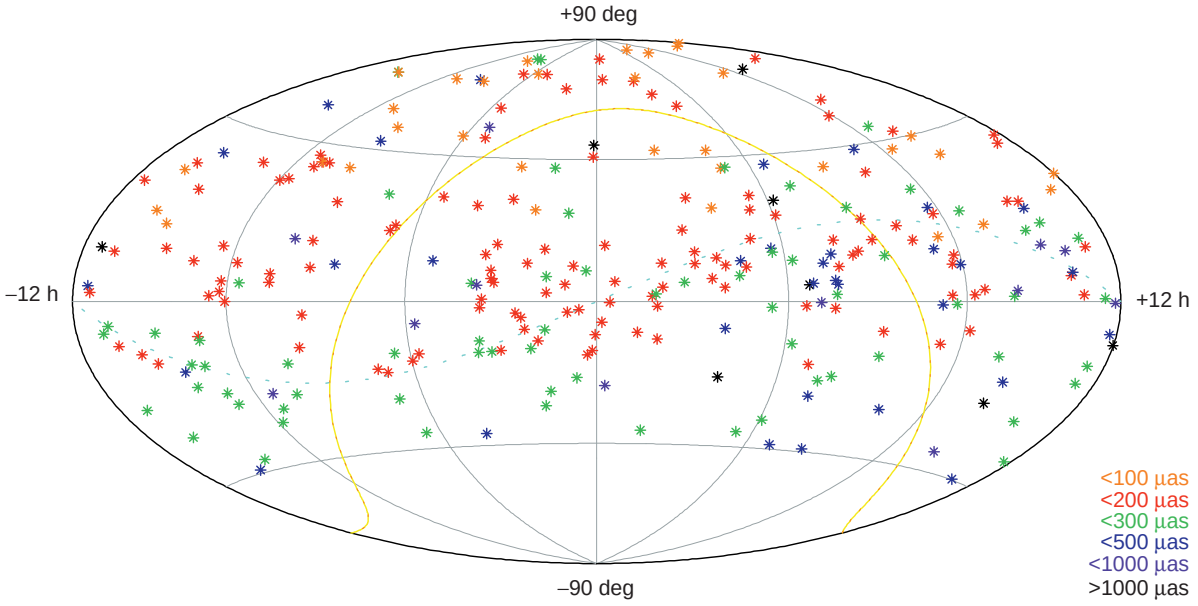

Fig. 4. Distribution of the 291 sources in JPL 1997-3 in an Aitoff equal area projection. The sources are color coded by the size of the declination formal error (μas). There are several items to note: (1) there is a systematic increase of declination uncertainties toward the south. In fact, because below δ = –20 deg sources can no longer be observed by the California–Spain baseline, there are no sources with formal errors ≤200 μas (orange and red) past this point; (2) there is a higher density of sources near the ecliptic plane (light-blue dashed line); (3) there is a lower density of sources near the galactic plane (yellow–orange dashed line) particularly near the galactic center, α = 17 h 45 m, δ = –29 deg; (4) the California station from the California–Australia baseline constrains observations to remain above δ = –45 deg; and (5) realistic errors are about twice the size of the color-coded formal errors.

especially likely for sources near the galactic center ($\alpha \approx 17$ hr 45 min, $\delta \approx -29$ deg), which also happens to be near the crossing of the galactic and ecliptic planes in the Southern Hemisphere. The failed observations of sources 1709−342, 1710−269, 1710−323, 1714−336, 1741−312, 1748−253, 1817−254, and 1829−106 are evidence of the difficulty of detecting extragalactic radio sources needed for spacecraft tracking in the far southern reaches of the ecliptic plane. Undetected sources that cannot be accounted for by the proximity of the galactic plane are listed at the end of Table 3. Observations of P 1342−104 and 2314+03 were attempted because of their proximity to the ecliptic plane (see the rightmost column of the table). Sources 3C 48 and 3C 286 were observed in order to help calibrate single-dish flux density measurements but were not sufficiently compact to be observed by the long baseline interferometer. In summary, the nondetection of many of the sources in Table 3 is thought to be understood.

Because the DSN has only one station in the Southern Hemisphere, the position uncertainties in the south typically are larger than those in the north. In particular, sources below −20 deg declination were observed on only one baseline (California–Australia). This circumstance not only results in larger formal errors, but it also leads to large correlations amongst the positions. For example, in the declination band from −20 deg to −45 deg, the median intersource correlation between a pair of declinations is $+45 \pm 13$ percent (uncertainty determined from the median absolute deviation). This band is particularly susceptible to zonal errors of a systematic nature arising from causes such as troposphere mismodeling. Minor errors in the troposphere delay model may cause zonal errors in this declination band of nearly 1 mas!

The overlapping observing programs of the Crustal Dynamics Project (CDP) [62] and the U.S. Naval Observatory [51] have yielded catalogs of similar quality but with coverage extended down to the south celestial pole. Sky coverage for these programs originally was extended below −45 deg with experiments conducted by the Naval Research Laboratory [85].

The internal precision of the JPL 1997-3 radio frame is given by median formal uncertainties of 123 μas in α scaled by $\cos\delta$ and of 188 μas in δ. Hereafter, we will simplify notation for errors in right ascension by using $\alpha\cos\delta$ to mean the error in right ascension scaled by $\cos\delta$. Figure 5 shows histograms of the formal uncertainties in $\alpha\cos\delta$ and δ. Table 4 lists for each of the 291 sources used in the JPL astrometric program the name, the right ascension, the declination, the formal coordinate errors, and the correlation between the right ascension and declination. It is conspicuous that the α–δ correlation coefficients are almost all negative. This occurs because the declination estimates are dominated by the geometry of just one baseline, California to Australia. Recall that the right ascension for the source GC 0235+16 was fixed in order to constrain the orientation of our frame. Its right ascension uncertainty, therefore, is zero in the 1997-3 solution. For use of this source as a calibrator, we provide an uncertainty $\sigma_\alpha = 0.00434$ ms inferred from a fit that was identical in all respects except for the substitution of OJ 287 as the right ascension reference.

Table 5 lists ancillary information for each of the 291 sources. The JPL source name is repeated, followed by the IAU name based on the source's position at Besselian epoch 1950 (B1950). Both naming conventions are given because both are frequently used in much of the literature on extragalactic radio sources. The names used in the new ICRF [63,64] are not given since they are implicit in the J2000 positions reported in Table 4. A more complete dictionary of aliases can be found in [63] or at http://hpiers.obspm.fr/webiers/results/icrf/dico.html. After the name, we tabulate the number of sessions in which the source was observed along with the number of observation pairs (delay, delay rate) included in our analysis. Lastly, we tabulate the mean epoch of observation along with the first and last epochs of observation. We recommend that any source listed with fewer than 3 sessions or 10 delay and rate observation pairs be considered to have a provisional position. Accordingly, the positions in this article for P 0238-084, GC 0250+17, 0405+305, GC 0459+06, P 1555-140, 2100+468, and DA 611 should be considered provisional. This precaution is necessary because such poorly observed sources are especially susceptible to having their position estimates biased by a single corrupted observation.

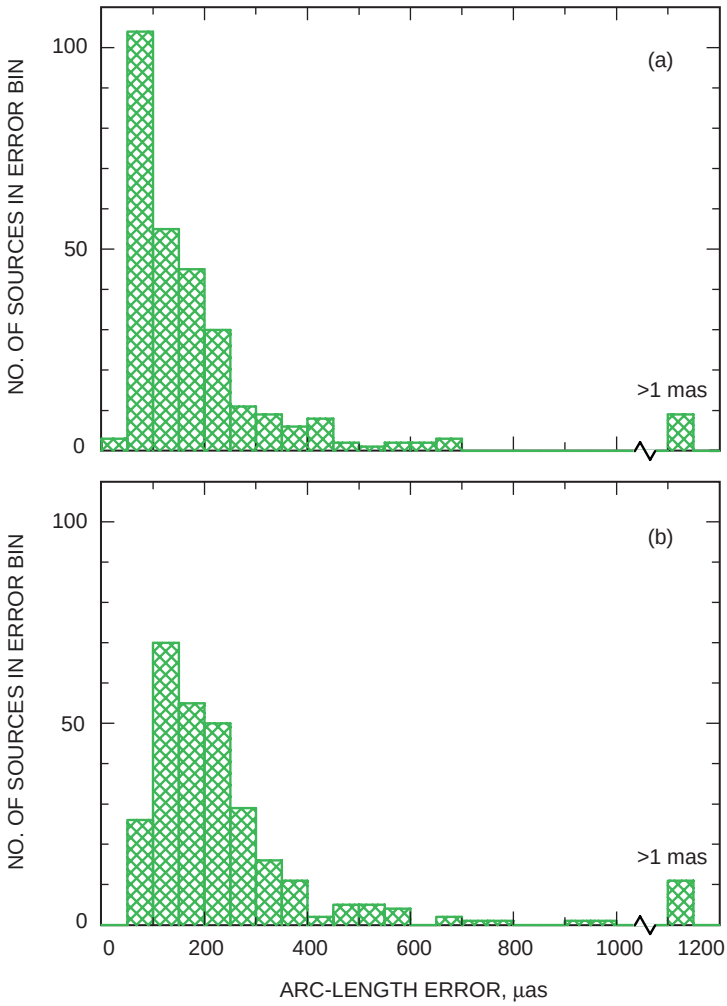

Fig. 5. Histogram of the 1997-3 formal position errors for 291 sources: (a) right ascension (scaled by cos δ) distribution with a 123-μas median and (b) declination distribution with a 188-μas median. Both DSN baselines have large east–west components, but only the California–Australia baseline has a large north–south component. Thus, the declination errors are larger than the right ascension errors. Realistic errors are about twice as large as the formal errors shown.

An examination of the full covariance matrix for the estimated coordinates shows large positive correlations amongst the declination coordinates. The median δ–δ correlation is $\approx$0.2. When one considers δ–δ correlations for just the declination band from $-$20-deg to $-$45-deg declination, the median correlation rises to 0.45! This is a result of having only one significant north–south baseline in our observing program. As a consequence, the declination estimates in this band are rather easily biased as a group. In other words, while differential declinations may be well determined, this southern declination band is susceptible to zonal errors in declination. We will attempt to quantify the level of zonal declination error in Section VII in the course of comparing our results with independent results. To remedy this situation, we hope to begin a series of experiments between Australia and South Africa to strengthen the geometry in the Southern Hemisphere.

Table 4. JPL 1997-3 extragalactic radio reference frame.

No.	Common source name	Right ascension			Declination			σ_α, 0.1 μs	σ_δ, μas	$\rho_{\alpha\delta}$
		hr	min	sec	deg	arcmin	arcsec			
1	0003−066	0	6	13.8929016	−6	23	35.333728	56	156	−0.1648
2	GC 0007+17	0	10	33.9906048	17	24	18.761856	76	157	−0.5266
3	P 0008−264	0	11	1.2467657	−26	12	33.375337	479	544	−0.8684
4	P 0013−00	0	16	11.0885622	−0	15	12.444260	68	164	−0.4185
5	0014+813	0	17	8.4748153	81	35	8.136790	565	116	0.0686
6	0016+731	0	19	45.7863749	73	27	30.017621	267	115	−0.1643
7	P 0019+058	0	22	32.4412216	6	8	4.270021	107	202	−0.7222
8	P 0048−09	0	50	41.3174000	−9	29	5.208892	67	172	−0.2453
9	P 0104−408	1	6	45.1080510	−40	34	19.958458	217	249	−0.2758
10	P 0106+01	1	8	38.7711162	1	35	0.318146	43	136	−0.1480
11	P 0111+021	1	13	43.1449719	2	22	17.317148	176	281	−0.8679
12	P 0112−017	1	15	17.0999777	−1	27	4.576165	46	142	−0.1347
13	P 0113−118	1	16	12.5219878	−11	36	15.432176	64	183	−0.1637
14	P 0119+11	1	21	41.5950479	11	49	50.413956	36	121	−0.2087
15	GC 0119+04	1	21	56.8617022	4	22	24.735293	46	138	−0.2494
16	DA 55	1	36	58.5947848	47	51	29.100745	65	92	−0.1059
17	0146+056	1	49	22.3708682	5	55	53.570188	137	234	−0.8120
18	P 0149+21	1	52	18.0590401	22	7	7.700601	43	111	−0.3584
19	0159+723	2	3	33.3849529	72	32	53.667916	297	118	0.0529
20	P 0201+113	2	3	46.6570686	11	34	45.410327	43	125	−0.3201
21	P 0202+14	2	4	50.4139150	15	14	11.043899	32	109	−0.1982
22	DW 0202+31	2	5	4.9253538	32	12	30.096083	77	119	−0.5455
23	0212+735	2	17	30.8133273	73	49	32.622424	192	80	0.0287
24	GC 0221+06	2	24	28.4281894	6	59	23.342569	47	130	−0.2977
25	DW 0224+67	2	28	50.0515041	67	21	3.029809	228	140	−0.0487
26	P 0229+13	2	31	45.8940527	13	22	54.716889	33	113	−0.1945
27	CTD 20	2	37	52.4056762	28	48	8.990489	37	93	−0.1979
28	GC 0235+16	2	38	38.9301113	16	36	59.275337	43	108	0.0000
29	GC 0237+04	2	39	51.2630487	4	16	21.412865	73	168	−0.5202
30	P 0237−23	2	40	8.1751032	−23	9	15.736448	1001	1155	−0.9545
31	P 0238−084	2	41	4.7985923	−8	15	20.751958	205	492	−0.6502
32	OD 166	2	42	29.1708552	11	1	0.728802	38	122	−0.2274
33	GC 0250+17	2	53	34.8822348	18	5	42.524992	409	1181	−0.3119
34	OD 094.7	2	59	27.0766329	7	47	39.644207	134	239	−0.7765
35	0259+121	3	2	30.5467708	12	18	56.750613	120	392	−0.4885
36	OE 400	3	3	35.2422058	47	16	16.276124	63	88	−0.0669
37	0302+625	3	6	42.6595347	62	43	2.024727	158	115	−0.1845
38	0306+102	3	9	3.6235277	10	29	16.341542	120	204	−0.7885
39	0309+411	3	13	1.9621137	41	20	1.184013	67	102	−0.2607
40	3C 84	3	19	48.1601386	41	30	42.105092	162	297	−0.2942
41	P 0317+188	3	19	51.2567433	19	1	31.290959	66	167	−0.5103
42	0326+277	3	29	57.6694089	27	56	15.499802	121	166	−0.7289

Table 4 (contd)

No.	Common source name	Right ascension			Declination			σ_α, 0.1 μs	σ_δ, μas	$\rho_{\alpha\delta}$
		hr	min	sec	deg	arcmin	arcsec			
43	P 0332−403	3	34	13.6545797	−40	8	25.396070	277	278	−0.4540
44	NRAO 140	3	36	30.1075888	32	18	29.342937	59	114	−0.2673
45	CTA 26	3	39	30.9378084	−1	46	35.802880	54	216	−0.2207
46	0341+158	3	44	23.1721668	15	59	43.370639	83	347	−0.2964
47	0342+147	3	45	6.4165428	14	53	49.558875	128	210	−0.8023
48	CTD 26	4	3	5.5860448	26	0	1.503285	55	145	−0.2968
49	P 0402−362	4	3	53.7499458	−36	5	1.911410	166	226	−0.1472
50	0405+305	4	8	20.3775251	30	32	30.489755	504	2222	0.8070
51	0406−127	4	9	5.7697426	−12	38	48.142743	142	254	−0.6411
52	GC 0406+12	4	9	22.0087159	12	17	39.848503	141	221	−0.8350
53	P 0420−01	4	23	15.8007380	−1	20	33.064388	52	147	−0.1668
54	VRO 41.04.01	4	23	56.0097753	41	50	2.713596	154	487	0.4944
55	P 0425+048	4	27	47.5704269	4	57	8.328185	695	1040	−0.9887
56	3C 120	4	33	11.0956069	5	21	15.619510	129	312	−0.5828
57	P 0434−188	4	37	1.4827472	−18	44	48.612171	82	195	−0.1615
58	P 0438−43	4	40	17.1799939	−43	33	8.601873	475	355	−0.6721
59	NRAO 190	4	42	38.6607540	−0	17	43.418966	250	666	−0.5776
60	0440+345	4	43	31.6352447	34	41	6.664042	257	287	−0.7998
61	P 0446+11	4	49	7.6711066	11	21	28.597227	110	344	−0.5276
62	P 0451−28	4	53	14.6468562	−28	7	37.326483	375	480	−0.8446
63	0454−234	4	57	3.1792583	−23	24	52.018832	106	219	−0.2671
64	P 0458−02	5	1	12.8098977	−1	59	14.255300	63	159	−0.2911
65	P 0458+138	5	1	45.2708385	13	56	7.221099	198	321	−0.8184
66	GC 0459+06	5	2	15.4459423	6	9	7.494954	284	514	−0.8482
67	0500+019	5	3	21.1971417	2	3	4.677939	144	261	−0.7491
68	P 0502+049	5	5	23.1847454	4	59	42.725191	273	469	−0.8642
69	0454+844	5	8	42.3636528	84	32	4.544425	506	71	−0.0215
70	P 0506+101	5	9	27.4570858	10	11	44.600714	62	141	−0.4369
71	P 0507+17	5	10	2.3691289	18	0	41.582305	121	192	−0.7931
72	P 0511−220	5	13	49.1143304	−21	59	16.090643	138	282	−0.4307
73	P 0528+134	5	30	56.4167445	13	31	55.149976	39	111	−0.1310
74	P 0537−441	5	38	50.3615169	−44	5	8.936773	392	325	−0.6007
75	P 0537−158	5	39	32.0101760	−15	50	30.319947	298	579	−0.7439
76	0536+145	5	39	42.3659995	14	33	45.562373	56	122	−0.3924
77	0544+273	5	47	34.1489417	27	21	56.842951	209	244	−0.8515
78	DA 193	5	55	30.8056044	39	48	49.165416	52	82	−0.0567
79	0556+238	5	59	32.0331385	23	53	53.927304	61	117	−0.4307
80	0600+177	6	3	9.1302831	17	42	16.811010	136	204	−0.8262
81	P 0605−08	6	7	59.6992466	−8	34	49.977216	65	187	−0.1513
82	P 0607−15	6	9	40.9495220	−15	42	40.671260	87	216	−0.2636
83	0611+131	6	13	57.6927635	13	6	45.402147	100	272	−0.5037
84	0615+820	6	26	3.0062797	82	2	25.567884	473	89	0.0144

Table 4 (contd)

No.	Common source name	Right ascension			Declination			σ_α, 0.1 μs	σ_δ, μas	$\rho_{\alpha\delta}$
		hr	min	sec	deg	arcmin	arcsec			
85	3C 166	6	45	24.0995135	21	21	51.202028	138	205	−0.7871
86	P 0646−306	6	48	14.0964943	−30	44	19.658454	323	378	−0.7495
87	0650+371	6	53	58.2828427	37	5	40.606845	62	105	−0.1585
88	0657+172	7	0	1.5255445	17	9	21.702106	46	107	−0.2176
89	OI 417	7	13	38.1640414	43	49	17.201493	347	365	−0.4169
90	0716+714	7	21	53.4485067	71	20	36.363591	188	96	−0.0320
91	P 0722+145	7	25	16.8077586	14	25	13.746918	136	391	−0.4686
92	DW 0723−00	7	25	50.6399471	−0	54	56.543446	204	332	−0.8578
93	P 0727−11	7	30	19.1124789	−11	41	12.599783	65	171	−0.0774
94	P 0735+17	7	38	7.3937547	17	42	18.998656	42	103	−0.1233
95	P 0736+01	7	39	18.0339110	1	37	4.618453	62	164	−0.2845
96	OI 363	7	41	10.7033185	31	12	0.228272	114	300	−0.1590
97	DW 0742+10	7	45	33.0595793	10	11	12.692066	78	162	−0.5166
98	P 0743−006	7	45	54.0823229	−0	44	17.539370	134	260	−0.6731
99	GC 0743+25	7	46	25.8741407	25	49	2.135135	162	335	−0.5233
100	B2 0745+24	7	48	36.1092822	24	0	24.110499	52	124	−0.2037
101	P 0748+126	7	50	52.0457351	12	31	4.828812	75	161	−0.5108
102	0749+540	7	53	1.3845786	53	52	59.637129	100	112	−0.0348
103	P 0754+100	7	57	6.6429395	9	56	34.851676	152	347	−0.6050
104	P 0805−07	8	8	15.5360379	−7	51	9.885547	63	178	−0.1292
105	P 0808+019	8	11	26.7073214	1	46	52.220783	55	145	−0.1800
106	OJ 425	8	18	15.9996100	42	22	45.414887	72	91	−0.1816
107	P 0823+033	8	25	50.3383615	3	9	24.520831	47	131	−0.0617
108	B2 0827+24	8	30	52.0861803	24	10	59.821133	136	258	−0.4513
109	OJ 448	8	32	23.2167148	49	13	21.037828	122	246	0.0512
110	0833+585	8	37	22.4097967	58	25	1.845380	217	158	0.0581
111	4C 71.07	8	41	24.3658545	70	53	42.172708	3393	1885	0.2308
112	OJ 287	8	54	48.8749274	20	6	30.641146	43	102	−0.1071
113	P 0859−14	9	2	16.8308980	−14	15	30.874212	84	207	−0.2426
114	OJ 499	9	3	3.9901093	46	51	4.137329	85	125	−0.1105
115	P 0906+01	9	9	10.0916049	1	21	35.618325	164	300	−0.7751
116	P 0912+029	9	14	37.9134715	2	45	59.246497	450	679	−0.9424
117	0917+449	9	20	58.4584854	44	41	53.984907	72	95	−0.0639
118	0919−260	9	21	29.3537754	−26	18	43.384212	1047	1142	−0.9502
119	P 0920−39	9	22	46.4182917	−39	59	35.067186	592	596	−0.8654
120	4C 39.25	9	27	3.0139007	39	2	20.851981	59	85	−0.0749
121	P 0925−203	9	27	51.8243249	−20	34	51.231375	182	361	−0.6148
122	AO 0952+17	9	54	56.8236344	17	43	31.222802	107	228	−0.5037
123	OK 290	9	56	49.8753797	25	15	16.049673	53	108	−0.2192
124	GC 1004+14	10	7	41.4980604	13	56	29.601530	155	590	−0.5005
125	1011+250	10	13	53.4287365	24	49	16.441382	58	141	−0.2402
126	1012+232	10	14	47.0654362	23	1	16.571113	291	354	−0.9074

Table 4 (contd)

No.	Common source name	Right ascension			Declination			σ_α, 0.1 μs	σ_δ, μas	$\rho_{\alpha\delta}$
		hr	min	sec	deg	arcmin	arcsec			
127	GC 1022+19	10	24	44.8095972	19	12	20.415752	102	228	−0.4653
128	P 1034−293	10	37	16.0797842	−29	34	2.812835	143	220	−0.2004
129	OL 064.5	10	41	17.1625068	6	10	16.924176	87	186	−0.4971
130	3C 245	10	42	44.6052277	12	3	31.263553	130	537	−0.3695
131	1039+811	10	44	23.0626580	80	54	39.442784	317	75	0.0127
132	P 1042+071	10	44	55.9112614	6	55	38.262861	136	368	−0.5143
133	1044+719	10	48	27.6199163	71	43	35.938261	208	111	−0.1136
134	P 1055+01	10	58	29.6052193	1	33	58.824096	52	139	−0.1299
135	P 1104−445	11	7	8.6941052	−44	49	7.617732	521	386	−0.7221
136	GC 1111+14	11	13	58.6951142	14	42	26.952883	176	285	−0.7739
137	P 1116+12	11	18	57.3014452	12	34	41.718264	57	162	−0.2287
138	P 1123+26	11	25	53.7119398	26	10	19.978446	52	100	−0.1484
139	P 1124−186	11	27	4.3924480	−18	57	17.440941	132	249	−0.5073
140	P 1127−14	11	30	7.0525874	−14	49	27.387503	114	309	−0.3661
141	GC 1128+38	11	30	53.2826316	38	15	18.546469	125	148	−0.5307
142	P 1130+009	11	33	20.0557982	0	40	52.837489	157	291	−0.7457
143	1144+402	11	46	58.2978991	39	58	34.304377	97	118	−0.3732
144	P 1144−379	11	47	1.3707646	−38	12	11.023052	159	231	−0.0604
145	1145−071	11	47	51.5540050	−7	24	41.139093	115	320	−0.4694
146	P 1148−00	11	50	43.8707727	−0	23	54.202828	144	911	−0.4168
147	1150+812	11	53	12.4992691	80	58	29.154239	313	77	0.0650
148	P 1156−094	11	59	12.7119240	−9	40	52.051417	1105	1534	−0.9882
149	GC 1156+29	11	59	31.8339125	29	14	43.826670	55	102	−0.1451
150	ON 231	12	21	31.6905011	28	13	58.500017	84	137	−0.4521
151	P 1222+037	12	24	52.4219457	3	30	50.293190	208	365	−0.8216
152	3C 273	12	29	6.6997739	2	3	8.599032	84	201	−0.4533
153	3C 274	12	30	49.4235830	12	23	28.041613	997	1376	−0.9865
154	1243−072	12	46	4.2321157	−7	30	46.573793	111	265	−0.4909
155	P 1244−255	12	46	46.8021041	−25	47	49.288548	122	222	−0.2662
156	P 1252+11	12	54	38.2556213	11	41	5.895184	73	170	−0.4049
157	3C 279	12	56	11.1665838	−5	47	21.524498	71	218	−0.2642
158	P 1302−102	13	5	33.0150293	−10	33	19.427132	74	197	−0.2349
159	B2 1308+32	13	10	28.6638482	32	20	43.782658	57	89	−0.1374
160	OP−322	13	16	7.9860539	−33	38	59.172470	151	230	−0.1726
161	OP 326	13	17	36.4941830	34	25	15.932326	81	128	−0.2663
162	1324+224	13	27	0.8613178	22	10	50.162866	52	101	−0.1982
163	DW 1335−12	13	37	39.7828128	−12	57	24.692720	67	175	−0.0935
164	1338+381	13	40	22.9517492	37	54	43.833964	192	432	−0.4019
165	GC 1342+662	13	43	45.9595417	66	2	25.744791	366	264	0.0168
166	GC 1342+663	13	44	8.6796713	66	6	11.643282	144	82	0.0665
167	P 1349−439	13	52	56.5350614	−44	12	40.387413	370	314	−0.5665
168	P 1354+19	13	57	4.4366561	19	19	7.372410	52	102	−0.2146

Table 4 (contd)

No.	Common source name	Right ascension			Declination			σ_α, 0.1 μs	σ_δ, μas	$\rho_{\alpha\delta}$
		hr	min	sec	deg	arcmin	arcsec			
169	OP−192	13	57	11.2450270	−15	27	28.786340	101	205	−0.3703
170	OQ 208	14	7	0.3943984	28	27	14.690424	121	168	−0.7195
171	P 1406−076	14	8	56.4812358	−7	52	26.666017	139	241	−0.6785
172	P 1413+135	14	15	58.8175022	13	20	23.713207	71	169	−0.3628
173	GC 1418+54	14	19	46.5973847	54	23	14.786432	211	357	−0.4196
174	P 1424−41	14	27	56.2976989	−42	6	19.437463	256	264	−0.3516
175	OQ−151	14	32	57.6906641	−18	1	35.247986	225	334	−0.7706
176	P 1435−218	14	38	9.4694961	−22	4	54.748083	177	289	−0.5768
177	1443−162	14	45	53.3763750	−16	29	1.618845	157	261	−0.6345
178	P 1445−16	14	48	15.0542242	−16	20	24.548795	142	249	−0.6028
179	OR 103	15	4	24.9798009	10	29	39.198696	49	112	−0.1788
180	1504+377	15	6	9.5299464	37	30	51.132265	95	164	−0.1561
181	P 1504−167	15	7	4.7870089	−16	52	30.266750	90	211	−0.2834
182	P 1510−08	15	12	50.5329687	−9	5	59.829238	64	164	−0.1440
183	P 1511−100	15	13	44.8934996	−10	12	0.264344	156	283	−0.6844
184	P 1514−24	15	17	41.8132120	−24	22	19.475499	168	256	−0.5332
185	P 1519−273	15	22	37.6761042	−27	30	10.785342	132	221	−0.2546
186	P 1532+01	15	34	52.4536915	1	31	4.206929	72	169	−0.3924
187	GC 1538+14	15	40	49.4915212	14	47	45.885037	58	119	−0.3557
188	P 1546+027	15	49	29.4368694	2	37	1.163788	56	164	−0.2127
189	DW 1548+05	15	50	35.2692614	5	27	10.448227	53	141	−0.2104
190	DW 1555+00	15	57	51.4339894	−0	1	50.413265	53	135	−0.1405
191	P 1555−140	15	58	21.9489503	−14	9	59.061909	3165	4193	−0.9961
192	B2 1600+33	16	2	7.2634547	33	26	53.072663	74	174	−0.1012
193	P 1604−333	16	7	34.7624268	−33	31	8.912504	234	282	−0.5334
194	P 1606+10	16	8	46.2032009	10	29	7.775904	99	170	−0.6803
195	DA 406	16	13	41.0642326	34	12	47.908637	61	106	−0.1818
196	P 1614+051	16	16	37.5568382	4	59	32.736761	97	226	−0.5108
197	P 1622−253	16	25	46.8917986	−25	27	38.326622	443	536	−0.8870
198	1624+416	16	25	57.6696741	41	34	40.629102	120	130	−0.4409
199	P 1622−29	16	26	6.0209955	−29	51	26.970980	219	289	−0.5810
200	GC 1633+38	16	35	15.4929582	38	8	4.500423	80	146	−0.1828
201	P 1637+574	16	38	13.4562398	57	20	23.978623	104	83	−0.0714
202	NRAO 512	16	40	29.6327478	39	46	46.028413	69	117	−0.0909
203	1642+690	16	42	7.8484301	68	56	39.756090	158	80	−0.0451
204	3C 345	16	42	58.8099583	39	48	36.994025	67	84	−0.2147
205	P 1647−296	16	50	39.5442420	−29	43	46.954235	250	320	−0.6680
206	DA 426	16	53	52.2166595	39	45	36.608744	107	137	−0.4710
207	OS 092	16	58	9.0114632	7	41	27.541401	67	168	−0.4002
208	DW 1656+05	16	58	33.4473686	5	15	16.444755	63	193	−0.3279
209	P 1657−261	17	0	53.1541344	−26	10	51.724422	140	232	−0.3753
210	OT−111	17	9	34.3454344	−17	28	53.364014	101	217	−0.3801

Table 4 (contd)

No.	Common source name	Right ascension			Declination			σ_α, 0.1 μs	σ_δ, μas	$\rho_{\alpha\delta}$
		hr	min	sec	deg	arcmin	arcsec			
211	GC 1717+17	17	19	13.0484813	17	45	6.438400	180	600	−0.3219
212	NRAO 530	17	33	2.7058288	−13	4	49.547066	67	173	−0.1304
213	1732+389	17	34	20.5785105	38	57	51.442807	68	91	−0.2573
214	OT 465	17	39	57.1290427	47	37	58.361412	219	340	−0.2808
215	4C 51.37	17	40	36.9777931	52	11	43.407371	92	99	−0.0122
216	P 1741−038	17	43	58.8561707	−3	50	4.616071	54	145	−0.1420
217	GC 1743+17	17	45	35.2081846	17	20	1.423432	51	148	−0.2390
218	1749+701	17	48	32.8402120	70	5	50.768393	779	401	−0.2075
219	OT 081	17	51	32.8185903	9	39	0.728586	47	129	−0.2147
220	GC 1751+28	17	53	42.4736223	28	48	4.938931	95	147	−0.5761
221	1803+784	18	0	45.6837885	78	28	4.018287	255	70	−0.0728
222	3C 371	18	6	50.6805418	69	49	28.108299	156	73	−0.0861
223	1826+796	18	23	14.1086459	79	38	49.002735	1138	292	0.2571
224	P 1821+10	18	24	2.8552834	10	44	23.773460	173	460	−0.5965
225	3C 390.3	18	42	8.9897629	79	46	17.127879	1318	296	−0.4320
226	3C 395	19	2	55.9388993	31	59	41.701728	136	213	−0.5074
227	OV−213	19	11	9.6529312	−20	6	55.107792	87	201	−0.2189
228	OV−235	19	23	32.1898691	−21	4	33.331958	86	202	−0.1906
229	OV−236	19	24	51.0560475	−29	14	30.119808	122	211	−0.1275
230	OV 239.7	19	25	59.6053717	21	6	26.162052	49	105	−0.3545
231	1928+738	19	27	48.4950890	73	58	1.569795	260	106	0.0233
232	1929+226	19	31	24.9167768	22	43	31.258754	72	199	−0.3475
233	P 1933−400	19	37	16.2175686	−39	58	1.552323	190	239	−0.1841
234	P 1936−15	19	39	26.6577730	−15	25	43.056969	136	240	−0.6021
235	1947+079	19	50	5.5395251	8	7	13.989088	287	548	−0.7539
236	1954+513	19	55	42.7382129	51	31	48.546281	85	99	−0.1150
237	OV−198	20	0	57.0904846	−17	48	57.671363	75	188	−0.1435
238	OW−015	20	11	14.2158905	−6	44	3.554657	719	1007	−0.9677
239	P 2008−159	20	11	15.7109733	−15	46	40.252373	81	191	−0.2433
240	2017+743	20	17	13.0791780	74	40	48.000097	262	99	0.0683
241	OW 637	20	22	6.6815831	61	36	58.804736	218	176	0.0337
242	2021+317	20	23	19.0173309	31	53	2.305758	72	193	0.0052
243	OW 551	20	31	47.9584849	54	55	3.140891	465	958	0.3715
244	P 2029+121	20	31	54.9942687	12	19	41.341283	148	350	−0.6468
245	3C 418	20	38	37.0346792	51	19	12.662742	102	138	0.0090
246	2051+745	20	51	33.7344075	74	41	40.498292	619	189	−0.5893
247	2100+468	21	2	17.0560049	47	2	16.253911	247	706	0.0886
248	P 2106−413	21	9	33.1886995	−41	10	20.603770	346	313	−0.5814
249	B2 2113+29B	21	15	29.4134352	29	33	38.367232	59	175	−0.2582
250	OX 036	21	23	44.5173460	5	35	22.094712	119	219	−0.7256
251	P 2126−15	21	29	12.1759234	−15	38	41.039340	109	228	−0.4359
252	P 2127+04	21	30	32.8774245	5	2	17.468739	314	762	−0.6379

Table 4 (contd)

No.	Common source name	Right ascension			Declination			σ_α, 0.1 μs	σ_δ, μas	$\rho_{\alpha\delta}$
		hr	min	sec	deg	arcmin	arcsec			
253	P 2128−12	21	31	35.2617630	−12	7	4.795233	102	214	−0.4363
254	P 2131−021	21	34	10.3096247	−1	53	17.238003	53	142	−0.2029
255	P 2134+004	21	36	38.5863982	0	41	54.213918	49	133	−0.1907
256	OX 161	21	39	1.3092717	14	23	35.992652	61	175	−0.3626
257	OX−173	21	46	22.9793494	−15	25	43.884048	109	221	−0.4419
258	OX 074	21	47	10.1630068	9	29	46.672537	103	197	−0.6972
259	P 2145+06	21	48	5.4586808	6	57	38.604938	44	121	−0.2231
260	OX 082	21	51	37.8754935	5	52	12.955417	116	205	−0.7550
261	2150+173	21	52	24.8193935	17	34	37.795552	67	181	−0.3881
262	OX−192	21	58	6.2819187	−15	1	9.326416	78	188	−0.2279
263	VRO 42.22.01	22	2	43.2913397	42	16	39.980235	60	87	−0.2268
264	B2 2201+31A	22	3	14.9757746	31	45	38.270333	67	121	−0.3794
265	P 2216−03	22	18	52.0377447	−3	35	36.878837	58	151	−0.2276
266	3C 446	22	25	47.2593088	−4	57	1.389505	61	155	−0.2394
267	P 2227−08	22	29	40.0843560	−8	32	54.434140	70	168	−0.2839
268	2229+695	22	30	36.4695914	69	46	28.077334	292	139	−0.1128
269	CTA 102	22	32	36.4089202	11	43	50.904670	47	120	−0.3302
270	GC 2234+28	22	36	22.4708541	28	28	57.413774	48	97	−0.3624
271	P 2233−148	22	36	34.0871679	−14	33	22.187867	118	234	−0.5073
272	OY−172.6	22	46	18.2319962	−12	6	51.276512	64	167	−0.1202
273	P 2245−328	22	48	38.6857997	−32	35	52.186212	183	245	−0.3823
274	3C 454.3	22	53	57.7479541	16	8	53.562007	51	118	−0.4128
275	P 2252−089	22	55	4.2398091	−8	44	4.020479	151	275	−0.7141
276	GC 2253+41	22	55	36.7077512	42	2	52.533283	273	225	−0.8409
277	GC 2254+07	22	57	17.3031385	7	43	12.303301	133	257	−0.7474
278	P 2254+024	22	57	17.5631022	2	43	17.512631	101	198	−0.6596
279	P 2255−282	22	58	5.9629315	−27	58	21.254815	176	248	−0.4797
280	GC 2318+04	23	20	44.8566154	5	13	49.953363	59	144	−0.4085
281	B2 2319+27	23	21	59.8622300	27	32	46.444619	76	285	0.0080
282	P 2320−035	23	23	31.9537735	−3	17	5.022792	55	151	−0.2126
283	P 2328+10	23	30	40.8522575	11	0	18.710325	92	178	−0.6789
284	2331−240	23	33	55.2378707	−23	43	40.656630	122	224	−0.3554
285	P 2335−027	23	37	57.3390958	−2	30	57.628352	77	184	−0.4492
286	P 2344+09	23	46	36.8385495	9	30	45.515731	157	254	−0.8495
287	P 2345−16	23	48	2.6085267	−16	31	12.020456	93	205	−0.3239
288	2351+456	23	54	21.6802324	45	53	4.237184	96	121	−0.1400
289	2351−154	23	54	30.1952184	−15	13	11.211622	79	188	−0.2316
290	DA 611	23	55	9.4582869	49	50	8.337362	3834	7118	−0.9887
291	P 2355−106	23	58	10.8824290	−10	20	8.610103	68	170	−0.2378

Table 5. JPL 1997-3 radio frame: ancillary data.

No.	JPL name	B1950 name	N_{sess}	N_{obs}	$T_{\rm mean}$	$T_{\rm first}$	$T_{\rm last}$
1	0003−066	0003−066	51	109	1993.101	1990.836	1995.923
2	GC 0007+17	0007+171	21	38	1993.334	1990.836	1995.203
3	P 0008−264	0008−264	19	40	1985.137	1979.970	1990.836
4	P 0013−00	0013−005	36	76	1992.959	1988.604	1996.044
5	0014+813	0014+813	5	14	1991.962	1991.263	1992.303
6	0016+731	0016+731	26	68	1992.992	1990.732	1996.281
7	P 0019+058	0019+058	41	85	1988.052	1982.499	1995.923
8	P 0048−09	0048−097	47	86	1992.066	1986.490	1995.904
9	P 0104−408	0104−408	33	80	1988.833	1978.825	1996.044
10	P 0106+01	0106+013	102	269	1988.022	1978.825	1996.041
11	P 0111+021	0111+021	43	93	1989.181	1979.970	1996.044
12	P 0112−017	0112−017	72	153	1992.230	1988.257	1996.041
13	P 0113−118	0113−118	41	86	1991.085	1978.825	1996.041
14	P 0119+11	0119+115	61	120	1992.191	1988.257	1995.923
15	GC 0119+04	0119+041	44	85	1990.899	1983.389	1995.923
16	DA 55	0133+476	77	200	1989.033	1979.000	1996.041
17	0146+056	0146+056	21	44	1991.208	1988.257	1995.923
18	P 0149+21	0149+218	47	96	1992.566	1988.385	1995.923
19	0159+723	0159+723	12	34	1992.842	1991.263	1994.214
20	P 0201+113	0201+113	53	110	1991.975	1983.268	1996.281
21	P 0202+14	0202+149	100	239	1989.633	1979.904	1996.281
22	DW 0202+31	0202+319	29	57	1992.855	1990.836	1995.923
23	0212+735	0212+735	51	179	1988.844	1982.910	1995.904
24	GC 0221+06	0221+067	47	100	1992.792	1988.257	1995.923
25	DW 0224+67	0224+671	22	49	1988.399	1979.904	1996.044
26	P 0229+13	0229+131	69	157	1992.555	1988.257	1996.281
27	CTD 20	0234+285	107	295	1989.068	1979.904	1996.281
28	GC 0235+16	0235+164	96	232	1988.926	1979.904	1996.281
29	GC 0237+04	0237+040	18	29	1992.568	1990.137	1995.808
30	P 0237−23	0237−233	17	26	1992.107	1979.970	1995.808
31	P 0238−084	0238−084	4	6	1993.562	1991.271	1995.203
32	OD 166	0239+108	76	170	1989.534	1982.499	1995.923
33	GC 0250+17	0250+178	3	3	1994.244	1992.973	1995.195
34	OD 094.7	0256+075	37	65	1988.284	1982.499	1995.923
35	0259+121	0259+121	11	25	1992.328	1987.356	1993.449
36	OE 400	0300+470	92	213	1989.425	1978.822	1996.281
37	0302+625	0302+625	29	79	1993.762	1991.978	1996.281
38	0306+102	0306+102	24	53	1992.462	1988.257	1995.923
39	0309+411	0309+411	42	85	1992.683	1986.493	1996.281
40	3C 84	0316+413	34	63	1989.712	1979.904	1995.904
41	P 0317+188	0317+188	17	36	1994.521	1992.877	1996.041
42	0326+277	0326+277	23	47	1992.399	1986.493	1995.923
43	P 0332−403	0332−403	32	70	1988.888	1978.825	1996.044
44	NRAO 140	0333+321	50	129	1986.093	1978.822	1993.449

Table 5 (contd)

No.	JPL name	B1950 name	N_{sess}	N_{obs}	$T_{\rm mean}$	$T_{\rm first}$	$T_{\rm last}$
45	CTA 26	0336−019	40	75	1988.954	1979.904	1996.041
46	0341+158	0341+158	11	26	1992.260	1988.637	1993.449
47	0342+147	0342+147	32	63	1990.737	1985.745	1995.923
48	CTD 26	0400+258	30	53	1992.527	1981.940	1996.041
49	P 0402−362	0402−362	52	126	1989.792	1979.000	1996.044
50	0405+305	0405+305	3	5	1993.449	1993.123	1994.101
51	0406−127	0406−127	25	41	1992.888	1987.005	1995.923
52	GC 0406+12	0406+121	62	131	1987.373	1979.904	1995.923
53	P 0420−01	0420−014	97	247	1989.721	1979.000	1996.281
54	VRO 41.04.01	0420+417	10	16	1984.115	1979.904	1991.271
55	P 0425+048	0425+048	26	51	1990.888	1986.490	1995.923
56	3C 120	0430+052	34	72	1987.679	1978.822	1993.334
57	P 0434−188	0434−188	88	186	1990.104	1979.970	1996.281
58	P 0438−43	0438−436	27	51	1987.247	1978.825	1996.044
59	NRAO 190	0440−003	8	12	1983.337	1979.000	1990.863
60	0440+345	0440+345	20	31	1991.778	1986.896	1995.203
61	P 0446+11	0446+112	9	17	1988.956	1988.260	1991.271
62	P 0451−28	0451−282	12	27	1988.374	1979.970	1992.836
63	0454−234	0454−234	32	63	1992.675	1990.732	1995.923
64	P 0458−02	0458−020	31	58	1992.596	1990.134	1995.808
65	P 0458+138	0458+138	19	24	1992.027	1986.896	1995.923
66	GC 0459+06	0459+060	5	7	1989.710	1988.598	1990.863
67	0500+019	0500+019	12	24	1990.164	1988.260	1992.227
68	P 0502+049	0502+049	7	10	1989.910	1988.598	1995.326
69	0454+844	0454+844	55	188	1990.381	1982.910	1996.281
70	P 0506+101	0506+101	45	84	1992.052	1986.896	1995.923
71	P 0507+17	0507+179	36	72	1991.622	1985.742	1996.041
72	P 0511−220	0511−220	14	18	1991.090	1987.005	1995.326
73	P 0528+134	0528+134	105	245	1989.293	1979.904	1996.281
74	P 0537−441	0537−441	34	66	1987.433	1978.825	1995.923
75	P 0537−158	0537−158	10	13	1991.030	1987.030	1995.203
76	0536+145	0536+145	52	97	1991.748	1986.490	1995.923
77	0544+273	0544+273	29	42	1990.923	1986.490	1995.923
78	DA 193	0552+398	108	327	1990.140	1978.822	1996.281
79	0556+238	0556+238	43	79	1990.827	1986.493	1995.923
80	0600+177	0600+177	44	87	1991.510	1985.742	1996.041
81	P 0605−08	0605−085	32	60	1991.532	1978.822	1995.904
82	P 0607−15	0607−157	26	46	1990.164	1979.000	1996.281
83	0611+131	0611+131	9	13	1990.753	1988.598	1991.496
84	0615+820	0615+820	22	51	1993.449	1991.263	1996.281
85	3C 166	0642+214	28	47	1991.712	1986.625	1995.923
86	P 0646−306	0646−306	12	26	1994.666	1993.118	1996.041
87	0650+371	0650+371	46	111	1993.058	1991.252	1996.281
88	0657+172	0657+172	64	157	1992.418	1985.742	1996.281

Table 5 (contd)

No.	JPL name	B1950 name	N_{sess}	N_{obs}	$T_{\rm mean}$	$T_{\rm first}$	$T_{\rm last}$
89	OI 417	0710+439	19	32	1993.318	1991.263	1995.904
90	0716+714	0716+714	14	43	1992.863	1991.266	1994.216
91	P 0722+145	0722+145	9	15	1989.121	1988.254	1991.263
92	DW 0723−00	0723−008	41	103	1986.323	1979.904	1995.921
93	P 0727−11	0727−115	99	256	1990.068	1978.822	1996.281
94	P 0735+17	0735+178	93	248	1990.321	1978.822	1996.281
95	P 0736+01	0736+017	21	47	1991.778	1988.254	1995.195
96	OI 363	0738+313	12	21	1987.211	1978.844	1992.303
97	DW 0742+10	0742+103	51	161	1985.479	1978.822	1993.334
98	P 0743−006	0743−006	26	41	1993.718	1991.263	1995.923
99	GC 0743+25	0743+259	9	19	1988.975	1988.254	1990.734
100	B2 0745+24	0745+241	42	110	1989.477	1983.266	1996.044
101	P 0748+126	0748+126	40	94	1986.685	1979.904	1995.923
102	0749+540	0749+540	22	54	1993.945	1991.266	1996.041
103	P 0754+100	0754+100	9	16	1989.181	1988.254	1990.734
104	P 0805−07	0805−077	29	73	1992.172	1987.005	1995.197
105	P 0808+019	0808+019	33	73	1993.997	1991.263	1996.281
106	OJ 425	0814+425	67	174	1990.285	1978.822	1996.284
107	P 0823+033	0823+033	97	251	1989.825	1979.896	1996.281
108	B2 0827+24	0827+243	12	19	1984.746	1979.896	1996.284
109	OJ 448	0828+493	8	23	1992.885	1991.263	1993.449
110	0833+585	0833+585	20	35	1993.901	1991.266	1996.041
111	4C 71.07	0836+710	7	15	1980.571	1979.901	1984.536
112	OJ 287	0851+202	103	303	1989.474	1978.822	1996.281
113	P 0859−14	0859−140	29	55	1991.301	1978.822	1996.044
114	OJ 499	0859+470	24	53	1991.660	1978.822	1993.449
115	P 0906+01	0906+015	6	16	1991.836	1991.263	1992.224
116	P 0912+029	0912+029	8	13	1989.167	1988.254	1990.734
117	0917+449	0917+449	34	96	1993.510	1990.134	1996.041
118	0919−260	0919−260	9	14	1992.683	1991.244	1995.923
119	P 0920−39	0920−397	12	18	1991.803	1987.005	1995.923
120	4C 39.25	0923+392	113	329	1988.962	1978.822	1996.281
121	P 0925−203	0925−203	9	19	1989.907	1987.005	1995.197
122	AO 0952+17	0952+172	18	28	1991.052	1979.896	1995.921
123	OK 290	0953+254	46	103	1993.192	1990.732	1996.281
124	GC 1004+14	1004+141	9	19	1982.767	1979.896	1990.734
125	1011+250	1011+250	27	55	1993.962	1991.266	1995.921
126	1012+232	1012+232	11	25	1989.781	1988.254	1992.224
127	GC 1022+19	1022+194	9	15	1989.989	1988.598	1990.740
128	P 1034−293	1034−293	57	154	1989.805	1979.896	1996.041
129	OL 064.5	1038+064	34	86	1985.951	1979.904	1992.836
130	3C 245	1040+123	8	12	1984.475	1979.896	1990.740
131	1039+811	1039+811	27	76	1993.255	1991.266	1996.281
132	P 1042+071	1042+071	9	17	1990.110	1988.254	1996.284

Table 5 (contd)

No.	JPL name	B1950 name	N_{sess}	N_{obs}	$T_{\rm mean}$	$T_{\rm first}$	$T_{\rm last}$
133	1044+719	1044+719	18	41	1992.770	1987.356	1996.281
134	P 1055+01	1055+018	105	278	1989.208	1979.896	1996.044
135	P 1104−445	1104−445	31	54	1988.598	1978.822	1996.041
136	GC 1111+14	1111+149	9	22	1984.754	1979.896	1990.578
137	P 1116+12	1116+128	18	41	1991.148	1980.033	1993.337
138	P 1123+26	1123+264	103	279	1989.307	1979.896	1996.284
139	P 1124−186	1124−186	18	36	1993.871	1992.202	1995.921
140	P 1127−14	1127−145	48	102	1988.219	1978.822	1996.284
141	GC 1128+38	1128+385	33	89	1986.447	1980.123	1995.921
142	P 1130+009	1130+009	15	27	1991.373	1979.904	1995.921
143	1144+402	1144+402	21	37	1993.195	1990.578	1996.041
144	P 1144−379	1144−379	61	178	1989.014	1978.822	1996.041
145	1145−071	1145−071	11	19	1989.833	1988.598	1990.740
146	P 1148−00	1148−001	15	24	1984.333	1978.822	1991.266
147	1150+812	1150+812	26	83	1992.948	1990.740	1996.281
148	P 1156−094	1156−094	13	21	1991.759	1987.005	1995.921
149	GC 1156+29	1156+295	46	99	1992.986	1990.740	1995.921
150	ON 231	1219+285	26	50	1992.836	1990.740	1995.921
151	P 1222+037	1222+037	33	64	1984.806	1979.896	1996.284
152	3C 273	1226+023	109	302	1988.456	1978.822	1996.041
153	3C 274	1228+126	9	17	1983.079	1979.896	1990.737
154	1243−072	1243−072	10	20	1989.986	1988.254	1990.740
155	P 1244−255	1244−255	62	142	1989.036	1979.896	1996.041
156	P 1252+11	1252+119	17	41	1993.732	1991.266	1995.921
157	3C 279	1253−055	58	136	1989.414	1978.822	1995.904
158	P 1302−102	1302−102	31	66	1992.022	1988.598	1995.904
159	B2 1308+32	1308+326	112	342	1989.208	1979.896	1996.284
160	OP−322	1313−333	46	117	1990.499	1978.822	1996.041
161	OP 326	1315+346	23	51	1992.445	1990.151	1996.041
162	1324+224	1324+224	51	136	1993.268	1991.471	1996.281
163	DW 1335−12	1334−127	105	256	1990.258	1978.844	1996.284
164	1338+381	1338+381	10	16	1994.548	1993.118	1996.041
165	GC 1342+662	1342+662	12	40	1985.332	1982.910	1996.281
166	GC 1342+663	1342+663	60	223	1988.178	1980.068	1996.281
167	P 1349−439	1349−439	33	66	1990.419	1980.074	1996.041
168	P 1354+19	1354+195	110	290	1989.274	1979.896	1996.284
169	OP−192	1354−152	42	76	1992.301	1988.254	1996.041
170	OQ 208	1404+286	31	64	1992.087	1988.238	1996.041
171	P 1406−076	1406−076	27	45	1992.522	1988.598	1995.921
172	P 1413+135	1413+135	18	37	1992.926	1991.266	1995.921
173	GC 1418+54	1418+546	25	102	1984.637	1980.120	1996.281
174	P 1424−41	1424−418	29	57	1993.008	1990.134	1996.041
175	OQ−151	1430−178	29	55	1989.474	1979.970	1995.921
176	P 1435−218	1435−218	27	43	1993.115	1990.740	1995.921

Table 5 (contd)

No.	JPL name	B1950 name	N_{sess}	N_{obs}	$T_{\rm mean}$	$T_{\rm first}$	$T_{\rm last}$
177	1443−162	1443−162	18	39	1992.246	1988.598	1995.921
178	P 1445−16	1445−161	27	56	1992.320	1988.598	1995.921
179	OR 103	1502+106	113	322	1989.003	1978.822	1996.284
180	1504+377	1504+377	11	30	1992.511	1990.134	1993.449
181	P 1504−167	1504−166	76	174	1990.159	1982.504	1996.281
182	P 1510−08	1510−089	95	254	1989.978	1978.822	1996.281
183	P 1511−100	1511−100	29	48	1992.055	1988.257	1995.921
184	P 1514−24	1514−241	27	53	1992.850	1988.257	1996.041
185	P 1519−273	1519−273	51	141	1989.345	1979.896	1996.041
186	P 1532+01	1532+016	26	50	1991.208	1988.254	1993.337
187	GC 1538+14	1538+149	35	83	1992.937	1990.578	1995.921
188	P 1546+027	1546+027	21	48	1993.137	1991.266	1995.904
189	DW 1548+05	1548+056	42	80	1991.641	1988.254	1995.904
190	DW 1555+00	1555+001	103	246	1990.052	1978.822	1996.281
191	P 1555−140	1555−140	8	8	1994.008	1992.224	1996.041
192	B2 1600+33	1600+335	9	29	1992.798	1990.578	1993.449
193	P 1604−333	1604−333	22	45	1993.726	1991.375	1996.041
194	P 1606+10	1606+106	19	42	1993.090	1990.578	1995.923
195	DA 406	1611+343	66	186	1988.798	1978.825	1996.281
196	P 1614+051	1614+051	11	19	1989.274	1986.627	1991.266
197	P 1622−253	1622−253	16	25	1993.060	1991.244	1995.808
198	1624+416	1624+416	28	48	1993.008	1990.134	1996.041
199	P 1622−29	1622−297	19	28	1992.943	1988.257	1995.808
200	GC 1633+38	1633+382	73	210	1987.797	1979.901	1996.281
201	P 1637+574	1637+574	33	119	1993.597	1990.740	1996.284
202	NRAO 512	1638+398	67	185	1986.932	1979.000	1996.281
203	1642+690	1642+690	26	73	1993.252	1990.732	1996.281
204	3C 345	1641+399	108	430	1987.501	1979.904	1995.923
205	P 1647−296	1647−296	16	25	1993.970	1991.471	1995.921
206	DA 426	1652+398	17	31	1993.929	1990.836	1996.041
207	OS 092	1655+077	22	55	1990.548	1985.748	1995.904
208	DW 1656+05	1656+053	23	52	1989.186	1979.896	1993.449
209	P 1657−261	1657−261	55	110	1990.151	1983.060	1996.041
210	OT−111	1706−174	47	108	1990.334	1983.060	1996.041
211	GC 1717+17	1717+178	8	24	1981.488	1979.904	1990.748
212	NRAO 530	1730−130	109	310	1989.389	1978.825	1996.041
213	1732+389	1732+389	49	113	1993.025	1990.836	1996.041
214	OT 465	1738+476	29	79	1986.189	1978.825	1996.044
215	4C 51.37	1739+522	37	97	1993.181	1990.578	1996.044
216	P 1741−038	1741−038	109	320	1989.699	1978.825	1996.281
217	GC 1743+17	1743+173	28	61	1993.049	1990.578	1995.904
218	1749+701	1749+701	23	99	1983.288	1979.901	1989.296
219	OT 081	1749+096	55	142	1991.471	1985.742	1996.281

Table 5 (contd)

No.	JPL name	B1950 name	N_{sess}	N_{obs}	$T_{\rm mean}$	$T_{\rm first}$	$T_{\rm last}$
220	GC 1751+28	1751+288	21	37	1992.844	1990.581	1996.044
221	1803+784	1803+784	35	100	1992.342	1988.385	1996.281
222	3C 371	1807+698	70	250	1987.501	1979.901	1995.904
223	1826+796	1826+796	12	26	1992.820	1991.266	1994.216
224	P 1821+10	1821+107	26	55	1985.918	1979.901	1996.281
225	3C 390.3	1845+797	6	13	1991.345	1990.732	1991.978
226	3C 395	1901+319	15	28	1993.901	1990.581	1995.923
227	OV−213	1908−201	70	145	1991.759	1983.060	1996.281
228	OV−235	1920−211	70	155	1991.814	1986.764	1996.281
229	OV−236	1921−293	57	178	1990.403	1978.825	1996.041
230	OV 239.7	1923+210	78	205	1992.167	1987.852	1996.281
231	1928+738	1928+738	30	77	1993.088	1990.732	1996.281
232	1929+226	1929+226	11	23	1993.726	1991.978	1995.904
233	P 1933−400	1933−400	32	82	1992.249	1979.970	1996.041
234	P 1936−15	1936−155	34	63	1992.109	1988.385	1995.923
235	1947+079	1947+079	19	26	1993.975	1990.581	1995.923
236	1954+513	1954+513	33	86	1993.249	1990.732	1996.281
237	OV−198	1958−179	98	234	1990.238	1978.825	1996.281
238	OW−015	2008−068	15	24	1993.159	1991.244	1995.137
239	P 2008−159	2008−159	46	87	1991.805	1988.257	1995.923
240	2017+743	2017+745	13	36	1992.874	1991.266	1994.216
241	OW 637	2021+614	26	63	1992.309	1985.742	1995.195
242	2021+317	2021+317	16	35	1993.170	1991.266	1995.137
243	OW 551	2030+547	7	13	1983.548	1979.901	1990.863
244	P 2029+121	2029+121	19	38	1984.888	1979.901	1991.271
245	3C 418	2037+511	13	31	1992.429	1990.732	1993.449
246	2051+745	2051+745	14	23	1992.844	1991.266	1994.216
247	2100+468	2100+468	1	6	1994.140	1994.140	1994.140
248	P 2106−413	2106−413	11	27	1995.085	1994.351	1996.041
249	B2 2113+29B	2113+293	58	123	1986.422	1979.901	1995.904
250	OX 036	2121+053	43	80	1991.129	1988.257	1995.923
251	P 2126−15	2126−158	21	37	1992.896	1990.836	1995.203
252	P 2127+04	2128+048	14	16	1993.052	1990.860	1996.041
253	P 2128−12	2128−123	46	81	1991.874	1988.257	1995.923
254	P 2131−021	2131−021	69	152	1992.202	1988.257	1996.281
255	P 2134+004	2134+004	102	234	1989.986	1978.825	1996.041
256	OX 161	2136+141	12	22	1992.811	1992.257	1993.449
257	OX−173	2143−156	22	36	1993.307	1990.836	1995.923
258	OX 074	2144+092	14	21	1992.653	1990.836	1995.203
259	P 2145+06	2145+067	101	287	1988.311	1978.825	1996.281
260	OX 082	2149+056	55	120	1987.047	1979.901	1995.808
261	2150+173	2150+173	18	33	1993.310	1990.836	1995.326
262	OX−192	2155−152	54	97	1990.430	1978.825	1996.281
263	VRO 42.22.01	2200+420	116	309	1989.384	1978.825	1996.281
264	B2 2201+31A	2201+315	38	65	1993.238	1990.740	1995.923

Table 5 (contd)

No.	JPL name	B1950 name	N_{sess}	N_{obs}	$T_{\rm mean}$	$T_{\rm first}$	$T_{\rm last}$
265	P 2216−03	2216−038	70	139	1989.899	1982.759	1996.281
266	3C 446	2223−052	61	131	1989.323	1982.499	1995.904
267	P 2227−08	2227−088	46	90	1992.109	1988.257	1995.923
268	2229+695	2229+695	18	41	1992.164	1985.745	1996.041
269	CTA 102	2230+114	104	254	1989.334	1978.825	1996.281
270	GC 2234+28	2234+282	106	269	1988.617	1979.901	1996.281
271	P 2233−148	2233−148	21	37	1993.614	1990.836	1995.923
272	OY−172.6	2243−123	108	236	1989.619	1978.825	1996.281
273	P 2245−328	2245−328	54	147	1989.540	1978.825	1996.044
274	3C 454.3	2251+158	87	225	1988.918	1978.825	1995.923
275	P 2252−089	2252−089	21	39	1993.115	1988.637	1995.808
276	GC 2253+41	2253+417	39	81	1986.921	1980.068	1995.923
277	GC 2254+07	2254+074	21	38	1991.858	1988.680	1995.923
278	P 2254+024	2254+024	26	52	1990.992	1988.257	1996.044
279	P 2255−282	2255−282	25	51	1993.463	1990.836	1996.044
280	GC 2318+04	2318+049	43	79	1991.827	1988.257	1995.904
281	B2 2319+27	2319+272	10	22	1992.478	1990.581	1993.449
282	P 2320−035	2320−035	95	198	1989.197	1979.901	1996.281
283	P 2328+10	2328+107	22	32	1992.577	1990.836	1995.923
284	2331−240	2331−240	30	54	1992.773	1990.836	1995.923
285	P 2335−027	2335−027	36	57	1992.451	1988.604	1995.923
286	P 2344+09	2344+092	18	29	1992.880	1990.836	1995.203
287	P 2345−16	2345−167	78	171	1991.074	1978.825	1996.281
288	2351+456	2351+456	26	46	1992.765	1990.137	1995.923
289	2351−154	2351−154	38	68	1991.989	1988.604	1994.693
290	DA 611	2352+495	2	2	1985.586	1979.901	1991.271
291	P 2355−106	2355−106	62	131	1991.468	1985.745	1996.044

VI. Accuracy: Internal Tests

Having presented estimated source positions along with their formal precisions, we now attempt to characterize the true accuracy of these positions. First, we will examine a number of tests of the internal consistency of our analysis. Internal tests include numerous examinations of the fit results for various aspects of the theoretical model related to station coordinates, nutation, instrumental stability, tides, plasma effects, relativistic effects, and troposphere. The numerical stability of the estimation algorithm and its computer implementation also are considered. Finally, the stability of the reference frame is examined in detail, in terms of time-dependent changes of both the individual source coordinates and global orientation. Comparisons to external standards of accuracy will be treated in Section VII.

The internal consistency tests indicate that, in addition to the formal uncertainties, there is evidence for systematic mismodeling at the level of a few hundred μas. Such systematic errors lead to estimates of realistic uncertainties that are approximately two times the formal uncertainties.

A. Consistency of Estimated Physical Parameters

1. Baseline Length Repeatability. The data were collected in a sparse series of day-long sessions spread over the period from late 1978 to early 1996. One test of the internal consistency of the analysis is to estimate a new vector baseline from each day's data. If, after modeling tidal effects, one may assume that the remaining station motion is linear due to tectonic drift of the continents, then the scatter of these estimates about a linear drift serves as a measure of the true level of error in our analysis. Note that the following results all reflect the a priori removal of a discontinuity due to the 1992 Landers earthquake. The Goldstone site is modeled as having moved in the summer of 1992 by -10, -16, and -1 mm in the local east, north, and vertical directions, respectively. Figure 6 shows the estimated session-by-session baseline length estimates. For the 79 sessions that used the California–Spain baseline, the best-fit linear drift was 14.8 ± 0.6 mm/yr with a value of $8,390,569.965 \pm 0.003$ m at epoch 1990.0. This drift accounts for tectonic motion with time. The wrms repeatability about this linear drift was

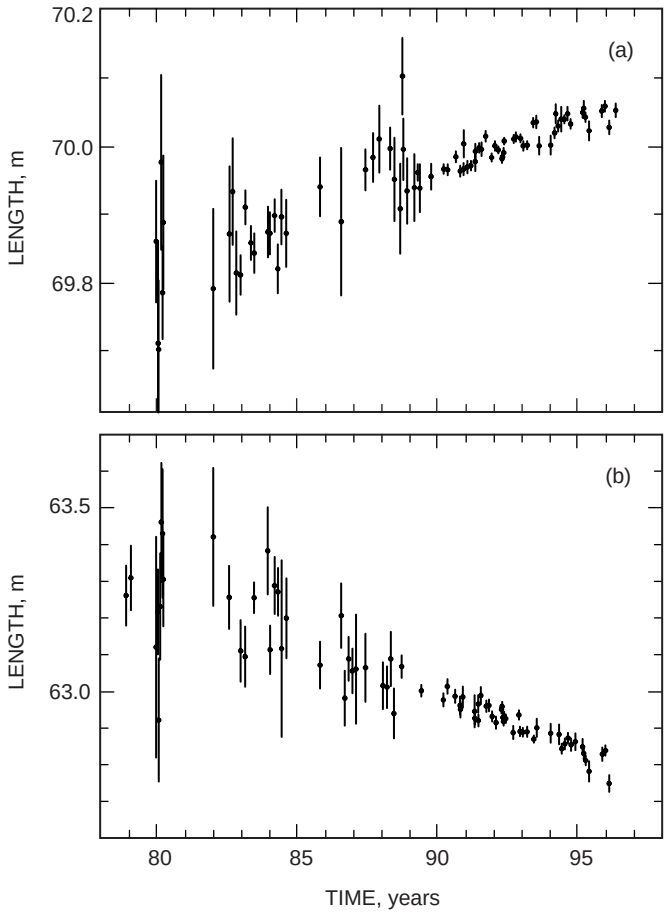

Fig. 6. Session-by-session baseline length estimates over the 17.5-year history of measurements: (a) California–Spain baseline length results (the wrms scatter about a linear drift is 13.0 mm with $\chi^2_\nu = 1.83 \pm 0.29$; the nominal length is 8,390,570 m with only the last few digits of the length shown) and (b) California–Australia baseline length results (the wrms about a linear drift is 23.8 mm with $\chi^2_\nu = 1.57 \pm 0.26$; the nominal length is 10,588,963 m with only the last few digits shown). Note the improvement in data quality c.1989 when the introduction of the MkIII recording system increased the recorded bit rate from 4 to 56 Mbits/s and the spanned bandwidth from 40 to 367 MHz.

13.0 mm with a $\chi^2_\nu = 1.83 \pm 0.29$. For the 75 sessions done with the California–Australia baseline, the best-fit linear drift was -31.1 ± 1.1 mm/yr with a value of $10,588,962.995 \pm 0.007$ m at epoch 1990.0. The wrms repeatability was 23.8 mm with a $\chi^2_\nu = 1.57 \pm 0.26$ where, again, a linear drift was removed. The assumption that baseline length changes should be linear due to tectonic motion was tested by comparing the Nuvel-1A tectonic motion model [20] with the observed changes. The model predicts a California–Spain drift of 16.5 ± 0.5 mm/yr and a California–Australia drift of -33.4 ± 1.0 mm/yr (we have assumed a 3 percent uncertainty in the Nuvel-1A rates), resulting in a 2σ level of agreement between model and experiment. Having thus validated the assumption of linear drift, we interpreted the excessive baseline scatters ($\chi^2_\nu > 1$) as evidence of unmodeled systematic errors at the level of ≈8.8 and ≈15 mm, on the Spain and Australia baselines, respectively. These baseline errors of 1 to 1.5 ppb correspond to systematic errors of roughly 200 to 300 μas in source positions.

2. Celestial Pole Position Repeatability. In a similar manner, the repeatability of the estimates of the celestial pole position ($\Delta\psi \sin\varepsilon, \Delta\varepsilon$) provide a measure of the true level of error in our analysis. The time series of pole positions for the 154 experiments was modeled to remove linear drifts and harmonic terms at 18.6-year, 9-year, annual, and semiannual periods for each pole coordinate in order to account for deficiencies in the a priori nutation model. The residual pole position estimates had wrms repeatabilities of 277 and 228 μas in ecliptic longitude and obliquity, respectively. The associated χ^2_ν was 5.04 ± 0.42. These tests indicate unmodeled systematic errors at the level of ≈250 μas. Note that Fig. 1 shows residual pole position estimates relative to the a priori model of Section IV.A, but before removal of the linear plus 18.6-, 9-, 1-, and 0.5-year terms just mentioned.

3. Mechanical and Phase Stability of the VLBI Instrument. The mechanical structures that support the reflecting surfaces of the antenna are not perfectly stable. We believe that the largest systematic instabilities are due to gravity loads and thermal expansion. As discussed in [90], antenna deformations due to gravity loads should be absorbed almost entirely into biases of the estimated station locations and clock offsets and, therefore, will have little effect on source positions. The effects of wind loading have not been examined carefully but are thought to have negligible effect on source positions ($\ll$100 μas). Since the temperature of an antenna has systematic diurnal and seasonal variations, thermal expansion is modeled for the vertical position of each antenna's reference point at the intersection of axes. We have not yet modeled the thermal expansion of the path through the antenna optics (primary and subreflectors). We estimate that this unmodeled portion of the delay varies by $\leq$10 ps for temperature excursions of 10 K. A test that omitted the modeling of the thermally induced vertical shift in the reference point resulted in source coordinates changing by $<$3 μas. We therefore conclude that any deficiencies in the thermal expansion model have negligible effects on source positions.

After traveling through the mechanical components of the antenna, the radio signal enters the antenna feed and passes through a series of amplifiers, filters, and cables. The phase variations of this signal path were continuously calibrated with the system designed by Sigman [87], who estimates the calibrations to be accurate to 10 ps over 24 hours (≈70 μas on long baselines). Averaged over many experiments, the net effect on source positions should be even smaller. Thus, we expect instrumental calibration instabilities to contribute 15 to 30 μas to source position errors. The calibration system itself is referenced to an H_2 maser atomic clock. Instabilities in this clock are another source of instrumental error. Tests that varied the interval between estimated clock offsets induced changes of ≈75 μas in astrometric parameters.

4. Tidal Effects: Love Numbers. To test the validity of our a priori solid Earth tidal models, we estimated the horizontal and vertical Love numbers, h and l. Small deviations from the standard values ($h = 0.609$ and $l = 0.0852$) were found at some of the antenna sites and were determined with approximate formal uncertainties of 0.004 and 0.001, respectively. These Love number shifts produced weighted mean offsets of -6 and 2 μas in $\alpha \cos\delta$ and δ, respectively. Also, the celestial coordinates were scattered by 14- and 16-μas wrms in right ascension and declination arc length, respectively. These changes are approximately 0.1 times the formal source position uncertainties and are considered a negligible change to the celestial reference frame.

5. Plasma Effects. The effects of charged-particle distributions on signal propagation have been calibrated using the standard dual-frequency technique (e.g., [91]). Because the effect of the Earth's magnetic field on the ionosphere's index of refraction [3] has been ignored, the dual-frequency calibration is expected to be in error at a level of $\leq$10 μas. An effect that is slightly smaller arises from a beam-mismatching effect. The antenna's S-band (13-cm) and X-band (3.5-cm) beams are in the far field when they intersect the ionosphere at an altitude of a few hundred kilometers. As a result, the conical beams differ in size according to the ratio of their aforementioned wavelengths. To the extent that stochastic variations of the ionosphere occur on scales as small as an S- or X-band beamwidth, the two beams will measure slightly different parts of the plasma, causing a miscalibration on the order of 1 ps. This amounts to a few μas for the long baselines under consideration here. A similar effect arises from the difference in refractive bending caused by the solar plasma. This refraction causes the S- and X-band rays to propagate along slightly different paths. This effect is thought to be small but has not been closely examined.

Since the effects of both the solar plasma and the Earth's ionosphere are greatest for ray paths nearest to the Sun, examining χ^2_ν as a function of angle from the Sun serves to test the assertion that plasma effects have been well calibrated. In fact, for the group delay observable, χ^2_ν shows no significant dependence on Sun angle. However, within the range 8 ± 5 deg of the Sun, the phase delay rates show a measurable increase in χ^2_ν to a value of 2.0 ± 0.14. Close examination of the data suggests that plasma-induced phase scintillations are causing 2π slips in the phase-tracking portion of the signal processing. Since these slips tend to occur simultaneously in all channels, the group delay ($\partial\phi/\partial\omega$) is relatively unaffected, while the phase rate ($\partial\phi/\partial t$) is seriously corrupted. As mentioned earlier (Section III.D), we made a concerted, albeit imperfect, attempt to identify and correct these cycle slip problems.

In order to assess the impact of the uncorrected cycle slips (and any other plasma mismodeling), a variation of the standard solution was made that eliminated all data within 10 deg of the Sun (0.64 percent of the data). The resulting source positions changed by 7-μas wrms in $\alpha\cos\delta$ and by 15-μas wrms in δ. Mean offsets of 1 and -10 μas in $\alpha\cos\delta$ and δ, respectively, were observed. The largest zonal error was 30 μas in $\Delta\delta$ versus δ. Since a fraction of the data were eliminated, the data strength of the solution is weakened so that some changes should be expected even in the absence of plasma mismodeling. Thus, one should attribute only a portion of the above changes to potential mismodeling. In summary, plasma errors are not a major part of the error budget at present.

6. Relativistic Effects. We have used Einstein's special and general theories of relativity to account for the relativistic effects on our observations. The errors in the relativistic modeling are expected to come not from errors in the theory per se, but rather from a failure to provide sufficiently accurate velocities and mass distributions, which are required as input parameters to the theories.

We tested the validity of our a priori gravitational retardation model by estimating the parameter γ_{PPN}, which characterizes the curvature of space–time produced by massive bodies (predominantly the Sun). In the parameterized post-Newtonian (PPN) approximation of general relativity, this parameter is equal to unity. Our estimate gave $(\gamma_{PPN} - 1) = 0.0011 \pm 0.0009$. The formal uncertainty of 9×10^{-4} is almost certainly optimistic, but understanding the contribution of all significant systematic errors to a more realistic uncertainty is beyond the scope of the present article. The consistency of our baseline ($\chi^2_\nu \approx 1.7$) and celestial pole estimates ($\chi^2_\nu = 5.0$) suggests that the realistic uncertainty probably is in the range of 0.0011 to 0.0020. One probable source of systematic error deserves a closer look. Observations near the Sun—where the gravitational effect is largest and where systematic error from solar plasma is largest—are expected to have the greatest potential for corrupting the estimate of γ_{PPN}. Thus, in order to test the robustness of this estimate, the solution was modified to exclude data within 10 deg of the Sun. This 0.64 percent reduction in the data altered the estimate of γ_{PPN} by -6×10^{-5}, thereby demonstrating its relative stability. The above result compares well with [81], $(\gamma_{PPN} - 1) = 0.0002 \pm 0.0020$, and [55], $(\gamma_{PPN} - 1) = -0.0004 \pm 0.0017$. Returning to the matter of source positions, fixing versus estimating γ_{PPN} created negligible mean offsets and scatters in source positions of $\leq$2 μas. All of these tests indicate that general relativity provides a good a priori description of gravitational retardation of radio signals.

Therefore, it was decided to fix γ_{PPN} to unity for the source coordinates reported in this article. Having argued that general relativity is a good model, we note that our implementation of that model is not complete. The present analysis models the gravitational effects of the Sun, the nine planets, and the Moon. The gravitational effects of the innumerable bodies lying between Earth and the distant extragalactic radio sources have not been modeled. In [43], these "microlensing" effects were estimated to be of the order of 10 μas in some average sense. The potential for a stochastic gravitational wave background to cause effects of a similar magnitude were investigated in [75].

A larger error exists in the special relativistic modeling because we have ignored the effect of the acceleration of the solar system barycenter (SSB) relative to the distant radio sources. Since the SSB's orbital period of ≈240 million years about the galactic center is much larger than the 17.5-year span of observations, the SSB velocity with respect to the extragalactic sources has been nearly constant. By assuming that this constant is zero, one implicitly absorbs a large (several arcmin) aberration effect into the reported source coordinates. This assumption is more a matter of convention than of error, and it is a convention consistent with all other published reference frames of which the authors are aware. However, as pointed out in [91], the SSB's acceleration toward the galactic center changes the velocity such that the aberration effect changes by as much as ≈5 μas/yr. This effect, when integrated over one-half the time span of the observations, amounts to ≈40 μas times the usual geometric projection factors for orbital aberration. Because the smallest reported formal errors in this article are ≈70 μas and because tropospheric mismodeling causes zonal errors >100 μas, this error may be considered negligible for the present. However, as the time span of observations increases and measurement accuracy improves, galactic acceleration of the SSB will need to be modeled.

7. Troposphere Mapping Function. The delay contribution from tropospheric refraction was modeled as an azimuthally symmetric function characterized by a delay at zenith and a "mapping" function that relates the zenith delay to the delay at a specified elevation, E, above the horizon. The mapping function scales as $1/\sin E$ plus some higher-order terms to account for the curvature of the Earth and the details of the atmospheric state as a function of height above the surface. To test the validity of our a priori troposphere modeling, we performed variant fits with two alternative high-quality mapping functions: the Lanyi [53] and the Niell [71] functions. For the 1997-3 frame, the Lanyi function was calculated using the U.S. Standard Atmosphere temperature profiles. These profiles also are used by the Niell function, although the formulation of the function differs from Lanyi. As a result, we can use these two functions to probe for deficiencies in their formulations. The wrms baseline length repeatability changed from 23.8 mm to 23.9 mm on the California–Australia baseline and from 13.0 mm to 14.2 mm on the California–Spain baseline when the mapping function was changed from the Lanyi to the Niell function. Source positions changed by <10-μas rms about a mean offset of only ≈1 μas for both coordinates. Zonal differences were a maximum of 40 μas in $\alpha\cos\delta$ versus δ and 20 μas in δ versus δ. In both cases, the maximum was at the southernmost declination observed, −45 deg. Thus, these alternative formulations, which start from the same temperature profile, induce little change in source positions other than a small zonal difference at far southern declinations.

8. Troposphere Temperature Profile. Next, we examined the consequences of inaccuracies in the assumed temperature profile. The Lanyi troposphere mapping function requires as input a model of the temperature profile as a function of altitude above the surface. It is particularly difficult to predict the tropospheric refractivity in the region from 2 to 10 km above the surface given only surface measurements. While the region from 2 to 10 km usually is well characterized by a smooth linear decrease in temperature versus altitude (lapse rate) of approximately −7 K/km, the lower region from 0 to 2 km is much less well behaved. Sometimes it has a linear lapse rate and at other times there are temperature inversions in which the temperature increases with altitude for the first kilometer or so. Thus, uncertainties in the 0- to 2-km region prevent accurate connection of the temperature profile from the surface to the 2- to 10-km region. In order to provide flexibility in treating this connection problem, the Lanyi function allows the analyst to specify a temperature profile as follows: a constant temperature from the surface up to an inversion height (≈0 to 2 km); thereafter, the temperature falls off at a linear lapse rate (≈ −7 K/km)

until, finally, above the tropopause height (≈9 to 15 km), the temperature is modeled as a constant. The main systematic error in modeling the hydrostatic component of the tropospheric delay may arise from errors in modeling this temperature profile. We compared two models: first, the U.S. Standard Atmosphere [18] as interpolated in [90]; second, profiles consisting of measured surface temperatures coupled with a 1.25-km inversion height, lapse rates of −7.2, −6.6, and −7.15 K/km, and tropopause heights of 11.5, 12.0, and 11.0 km, where the triplets of numbers apply to the California, Australia, and Spain antenna sites, respectively. The wrms scatter between the source positions derived from the two models is 44 μas in $\alpha \cos\delta$ and 27 μas in δ after removing weighted mean offsets of 5 μas and −30 μas, respectively. Perhaps of greater interest is the 200-μas peak-to-peak zonal change seen in $\alpha \cos\delta$ versus δ, which is of comparable size to the formal errors. Thus, it is estimated that errors in modeling the temperature profile may cause ≤30 μas random errors and ≤200 μas zonal systematic errors.

9. Troposphere Gradients. Another known limitation to our troposphere modeling is the assumption that the troposphere is azimuthally symmetric about the station [32,13,65]. Recent work (e.g., [64]) gives evidence from VLBI using large networks of antennas that this assumption causes a zonal error that is described as a 400-μas shift in declinations at the equator smoothly falling off to nearly zero toward both poles. The data analyzed for this article differ from the above cited works in that there are only single baselines that are very long (>8,000 km) rather than large multibaseline networks with a variety of baseline lengths. This circumstance restricts the range of azimuths that may be observed. At the Australia site, observations ranged over ≈120 deg of azimuth; at the Spain site, the range was ≈120 deg most of the time with an extended range of 180 deg being observed only once every 3 or 4 hours. The California site had ranges that were comparable to those of its overseas partner on a given day. These limited ranges result in two somewhat balancing and related effects: first, the small range reduces the need to account for changes as a function of azimuth; second, the narrow range reduces the geometric strength of the data that would be needed to estimate azimuthal asymmetry corrections directly from the data themselves. Thus, we expect that our azimuthally symmetric troposphere parameters absorb the average asymmetry over the limited sectors that are observed.

To test these assumptions, a variant of the standard analysis was made in which troposphere asymmetry was estimated (from the MkIII subset of our data) as a pair of east–west and north–south "gradient" parameters [32] for each session. This test produced weighted mean offsets of 8 and 256 μas in $\alpha \cos\delta$ and δ, respectively. Also, the celestial coordinates were scattered by 67- and 207-μas wrms in right ascension and declination arc length, respectively. The maximum zonal differences were 500 μas in $\Delta\alpha \cos\delta$ versus δ and 700 μas in δ versus δ. There was relatively little variation in position shifts as a function of α. Baseline repeatability changed on the California–Spain baseline from 11.3 to 13.2 mm (χ^2_ν changed from 2.31 to 1.51) and on the California–Australia baseline from 20.1 to 29.8 mm (χ^2_ν changed from 1.74 to 2.78). It is difficult to determine the proportion of these changes that may be attributed to a weakening of the solution from estimating poorly determined parameters as opposed to changes that are due to truly improved modeling. The repeatability of daily celestial pole positions was relatively unaffected. In contrast to the baseline and celestial pole repeatability, the source positions were improved when troposphere gradients were estimated. This was judged by comparing the "with" and "without" gradient solutions to the G-1069 reference frame from Goddard Space Flight Center. While little change was seen in right ascensions, the declination agreement improved from a scatter of 388- to 287-μas wrms and from a mean offset of 299 to 20 μas. Since the GSFC analysis also chose to estimate gradients, it is possible that the improved declination agreement is due in part to our after-the-fact decision to match the GSFC analysis choices. In summary, the evidence from our tests is mixed as to whether gradients improve the analysis or not. At the very least, one must be aware that this effect may cause large zonal differences as a function of declination.

Much further work remains to be done in this area. Our preliminary analysis of a larger multibaseline data set more strongly favors the estimation of gradients. However, even with such a geometrically strengthened data set, there are some troubling results. For example, the gradients estimated from pairs of antennas that are but a few kilometers apart (e.g., DSS 15 and Mojave, Kokee and Kauai, and

Haystack and Westford) show mean north–south gradients that are very repeatable for each antenna but statistically inconsistent with the antenna a few kilometers away. Since one of these antennas, DSS 15, was used in the great majority of our observations, it is important to understand the accuracy with which its gradients may be modeled. Further evidence concerning gradients comes from [13], which found that gradients estimated from coarse-resolution meteorological data and from VLBI are 60 percent correlated. While this is a positive step toward accounting for VLBI estimates of gradients, it suggests that the effect is not fully understood. Variations in local topography have not yet entered VLBI models and may explain some of the inconsistencies seen to date. For all these reasons, it was decided not to estimate gradients in our standard analysis.

B. Numerical Stability of Least-Squares Estimation

Once the a priori model has been subtracted from the observations, a linear least-squares fit adjusts the selected set of parameters in order to minimize the residual group delays and phase delay rates. The code that accomplishes this task is susceptible to numerical instabilities and coding errors. To guard against numerical instabilities, we implemented a square root information filter (SRIF) (e.g., [5]) in our software. The matrix inversion for the 1997-3 solution had condition numbers (roughly the ratio of largest to smallest eigenvalue of the least-squares matrix of the normal equations), which we estimated to be in the range of 10^5 to 10^8. The computation was done with Digital Equipment Corporation's VMS 6.2 operating system and an Alpha 600 5/333 workstation that provides almost 16 decimal places of accuracy (53 binary bits). The numerical noise thus is expected to be $\leq(10^8/10^{16}) = 10^{-8}$ of the estimated parameter shifts from their a priori values. A priori values of the 3491 estimated parameters are quite accurate in most cases, and the expected noise of one part in 10^8 of the change from the a priori value has a negligible effect on the source coordinates. This fact was verified by feeding back the estimated parameters for use as a priori values in a second iteration of the linearized least-squares fit.

In order to guard against possible computer hardware and/or compiler errors, we ran our analysis on two different computer architectures: Digital Equipment Corporation's 64-bit reduced-instruction-set computer (RISC) architecture workstation (Alpha model 600 5/333) and their 32-bit complex-instruction-set computer (CISC) architecture workstation (VAX 4000 model 90). Source positions in the two analyses differed at most by 1 and 2 μas in right ascension and declination, respectively. Average scatters and biases were much smaller than 1 μas. While this comparison does not eliminate the possibility of systematic errors that are common to both systems, it does test the numerical stability of the analysis on two very different computer architectures.

C. Source Stability: Apparent Proper Motions

Moving on to the question of reference frame stability, we consider the apparent proper motions of individual sources relative to the frame as a whole. These motions are of particular concern in applications that use a small number of objects selected from the reference frame. Examples of these types of applications are spacecraft navigation, occultations of radio sources, and measurements of pulsar positions in the radio frame; these will be discussed in more detail in Section IX.

In order to assess source position stability, we modified the 1997-3 reference frame solution to estimate linear time rates of change in right ascension, $\dot{\alpha}$, and declination, $\dot{\delta}$. The net rotation of the frame was constrained by fixing to zero the rates of change of three coordinates of well-observed sources ($\dot{\alpha}$, $\dot{\delta}$ of OJ 287, and $\dot{\delta}$ of CTD 20) along with the coordinate rates of change for 75 other sources that were judged to be too poorly observed (either <20 observations or <5-year time span) to determine meaningful rates. OJ 287 and CTD 20 were chosen in part because of their lack of structure on milliarcsecond scales, as indicated by the maps that Charlot [10] made from epoch 1985 data. These constraints augment the single constraint on the right ascension of GC 0235+16 that was imposed on the standard solution. Coordinate rate estimates are made only for sources with more than 20 observations distributed over at least 5 years. These criteria are satisfied by 214 of the 291 sources included in the 1997-3 reference frame. Median rate

formal uncertainties are 55- and 70-μas/yr in $\dot{\alpha}\cos\delta$ and $\dot{\delta}$, respectively. They indicate the limit of the data sensitivity to individual apparent proper motions.

Supplementary analysis verified that there are no biases or net rotation rates in the set of estimated source rates at the 20-μas/yr level. This result confirmed that the imposed rotational rate constraints enforced the stability of our solution as expected. Global motion of the celestial frame with respect to the terrestrial frame was characterized by applying an a priori precession/nutation model (cf., Section IV.A) and then, relative to this model, estimating celestial pole offset parameters as shown in Fig. 1. The source rate statistics described above are summarized in Table 6.

Details concerning the motions of some individual sources are given in Tables 7 and 8. Table 7 shows the seven most significant ($>4\sigma$) right ascension rates $\dot{\alpha}\cos\delta$. Similarly, Table 8 shows the seven most significant ($>4\sigma$) declination rates, $\dot{\delta}$, in units of μas/yr. Also given are the number of observations per source, $N_{\rm obs}$; the time span of the observations in years; the formal uncertainties in the rates, $\sigma_{\dot{\alpha}}$ and $\sigma_{\dot{\delta}}$; and the normalized rates, $\dot{\alpha}/\sigma_{\dot{\alpha}}$ and $\dot{\delta}/\sigma_{\dot{\delta}}$.

Table 6. JPL 1997-3 source rate statistics.

Coordinate	Median σ, μas/yr	wrms, μas/yr	Mean, μas/yr	χ^2_ν
$\dot{\alpha}\cos\delta$	55	73	23 ± 5	3.6 ± 0.3
$\dot{\delta}$	70	90	-10 ± 6	3.0 ± 0.3

Table 7. Most significant right ascension rates.

No.	Source	Span, yr	N_{obs}	$\dot{\alpha}$, μas/yr	$\sigma_{\dot{\alpha}}$ μas/yr	$\lvert\dot{\alpha}/\sigma\rvert$
1	OK 290	5.6	103	−208	33	6.2
2	P 1127−14	17.5	102	−503	80	6.2
3	0650+371	5.0	111	−280	47	6.0
4	OX−192	17.5	97	−302	58	5.2
5	4C 39.25	17.5	329	129	25	5.1
6	3C 273	17.2	302	165	35	4.7
7	1954+513	5.6	86	−216	53	4.1

Table 8. Most significant declination rates.

No.	Source	Span, yr	N_{obs}	$\dot{\delta}$, μas/yr	$\sigma_{\dot{\delta}}$ μas/yr	$\lvert\dot{\delta}/\sigma\rvert$
1	OX−192	17.5	97	380	62	6.1
2	OK 290	5.6	103	253	47	5.4
3	P 1127−14	17.5	102	443	91	4.9
4	B2 2201+31A	5.2	65	313	71	4.4
5	P 1435−218	5.2	43	−899	205	4.4
6	0259+121	6.1	25	2016	495	4.1
7	OX 036	7.7	80	653	163	4.0

It may be seen that the sources with the most significant apparent motion in right ascension are among those most frequently observed by the DSN. The term *apparent* proper motion is used because changes in a source's brightness distribution (or structure) can shift the effective brightness centroid of a source and, thus, its measured position even if the source's core remains fixed. As a case in point, 4C 39.25 with 329 observations spread over 113 sessions is a very frequently observed source and shows a 5.1-σ apparent proper motion of $\dot{\alpha} = 129 \pm 25$ μas/yr during the period from 1978 to 1996. This source is known to have significant structure (e.g., [36,10]). In all, a total of 19 $\dot{\alpha}$ and 15 $\dot{\delta}$ exceeded three times the formal uncertainty. These counts fall to 5 and 2, respectively, if the threshold is increased to 5σ. In summary, the apparent proper motions estimated from our data are probably more an indication of changing source structure than of true proper motion of the radio source cores. If these estimates reflect source structure changes, it must be noted that they represent average linear changes in source structure over time spans as long as 17.5 years. For the well-mapped source 4C 39.25, the significant component of apparent motion corresponds to the direction of large time-dependent changes in the source structure. We currently are investigating whether there may be large (>200-μas/yr) sporadic saw-tooth-like motions over shorter time spans that average down over longer time spans. Thus, we reiterate that our estimates for the stability of individual sources are averages over times scales of 5 to 18 years.

D. Global Stability: Precession and Nutation

We now turn our attention away from the stability of individual sources to consider the stability of the frame as a whole. In order to make the best use of the inherent angular stability of the radio frame, one must be able to relate the positions of the VLBI receiving stations (which are slowly moving in a frame rotating with the Earth) to the inertial radio frame. Thus, for many applications, the usable stability of the extragalactic radio reference frame is limited by the accuracy with which the motion of the Earth's celestial ephemeris pole (CEP) can be theoretically modeled or empirically parameterized. At present, this accuracy is limited by the accuracy of the precession constant and the amplitude of the long-term (18.6-year period) nutation inferred from the data. Modifying our standard solution to solve directly for the luni–solar precession constant (as well as the major nutation terms) yielded a correction to the IAU value of precession of -2941 ± 15 μas/yr. The formal uncertainty of 15 μas must be inflated by a factor of 2 or 3 to arrive at a more realistic error. The most uncertain component of the 18.6-year nutation amplitude had a formal error of 166 μas. A more detailed discussion of the ability of VLBI to measure the motion of the CEP is given in [12]. Since our VLBI data cover 17.5 years of the 18.6-year nutation cycle, the precession and 18.6-year nutation are well separated. However, one component of the 18.6-year nutation still is correlated to a component of the 9-year nutation at the 88 percent level. Thus, the motion of the CEP is known—within the span of our observations—to within a few hundred μas, and with a long-term stability of better than 100 μas/yr.

Another test of the validity of CEP modeling is provided by comparison of results of two different methods of inferring the motion of the CEP: first, direct estimation of the precession amplitude along with the amplitudes of the major nutation terms (in addition, the baseline was forced to follow a linear motion); second, estimating session-by-session corrections to $\Delta\psi \sin\varepsilon$ and $\Delta\varepsilon$ (see Fig. 1)—the standard solution. These two methods produced mean offsets of -46 and -205 μas and wrms scatters about these offsets of 154 and 222 μas in $\alpha \cos\delta$ and δ, respectively. The direct estimation method yielded a correction of -2941 ± 15 μas/yr to the IAU value of precession. Fitting a precession parameter (plus 18.6-, 9-, 1-, and 0.5-year terms) to the session-by-session CEP offsets yielded a correction of -2955 ± 19 μas/yr to the IAU value of precession. Thus, the estimate of the luni–solar precession constant is stable at the 1-σ level.

Lastly, we note the importance of using an accurate a priori nutation model. In addition to the primary analysis that used the ZMOA 1990-2 nutation model [39], two alternate analyses also were made: one using the IERS96 nutation series [66] and the second using the IAU 1980 series [101,86]. In all three cases, the a priori model was supplemented by estimating offsets to the CEP position for each session. While the IERS96 model altered source positions by less than 20-μas wrms, the IAU 1980 series caused

differences of more than 100-μas wrms. This demonstrates that daily estimates of CEP offsets are not able to compensate fully for deficiencies in a poor a priori nutation model such as the IAU 1980 series. Note that, compared with the IAU 1980 series, the ZMOA 1990–2 series has twice as many terms, and the IERS96 series has more than four times as many terms. Many of these "extra" terms have periods that are separated by much less than a day. Thus, we conjecture that daily CEP offsets are not able to model the high-frequency (sub-daily period) variations in CEP position caused by the beating of the numerous harmonic terms in the two larger nutation series.

E. Summary of Internal Consistency Tests

The tests documented in the preceding paragraphs have considered various potential sources of systematic error. The results of these tests are summarized in Table 9, which serves as a systematic "error budget." This budget is useful both for evaluating the accuracy of the 1997-3 reference frame and for guiding future efforts to improve the VLBI technique. Tests of mismodeling of particular effects are listed first in the table, whereas the last three items characterize the overall level of systematic error rather than an individual component of the error budget. The troposphere causes the largest errors. Persistent north–south refractivity gradients (azimuthal asymmetry) may cause zonal errors as large as 500 μas in the southern celestial hemisphere. Water vapor turbulence is estimated to cause $\approx$150 μas of error. Mapping function approximations and temperature profile mismodeling generally cause smaller errors, although profile errors may cause zonal errors as large as 200 μas for far southern declinations. Source structure errors vary widely. For most sources, this is not a dominant error, but for a small fraction of sources—perhaps 10 percent—it is the dominant error (see Tables 1 and 2). Among instrumentation errors, atomic clock instabilities may contribute as much as 75 μas; receiver sensitivity and phase stability each contribute about 35 μas; and thermal expansion mismodeling is thought to be negligible. A priori nutation and tidal mismodeling each contribute $\approx$20 μas. Plasma mismodeling may contribute 10 μas and relativistic mismodeling 10 to 40 μas. Numerical errors are thought to be negligible. Next, baseline and celestial ephemeris pole wrms repeatabilities of $\approx$250 μas are given as internal measures of the total error budget. For convenience, two external measures of the total error budget are given (in anticipation of the section to follow) that show the accuracy to be $\approx$325 μas. Lastly, an estimate of "analyst" error is given. It results from differences in analyses made by different experienced analysts.

VII. Accuracy: External Tests

In addition to the internal consistency tests discussed in Section VI, numerous external tests are possible for assessing the accuracy of the JPL 1997-3 reference frame. Comparisons with independent software packages enable us to evaluate the implementations of the theoretical models within JPL's MODEST software. Likewise, the results of independent astrometric observation and analysis programs can be compared with our results to infer realistic error levels from differences in data sets and analysis methods.

A. Differences in Modeling Software

The software used to analyze VLBI data is of necessity very complex. In particular, the code that models the theoretical group delay and phase delay rates includes numerous lengthy calculations. To guard against potential errors in the implementation of these models in our software, we compared the JPL VLBI modeling software to two other VLBI software packages. It needs to be stressed that such tests examine only the accuracy of implementing a given set of models, without consideration of the inherent accuracy of the models themselves.

JPL's MODEST modeling software [90] was compared to Goddard Space Flight Center's CALC software[9] [79,60] and Paris Observatory's GLORIA software [33]. We used the two experiments done

[9] D. Gordon, Goddard Space Flight Center, Greenbelt, Maryland, 1985.

Table 9. Error budget: a summary of systematic error tests.

No.	Description	Error, μas
	Error budget components	
1	Troposphere:	
	Water vapor turbulence	150
	Temperature profile	30–200
	Mapping function formulation	1–30
	Azimuthal asymmetry	5–500
2	Source structure	0–1000
3	Instrumentation:	
	Receiver sensitivity (SNR)	35
	Atomic clock stability	75
	Instrumental calibration	35
	Antenna mechanical stability	10
4	A priori nutation model	20
5	Tides	20
6	Plasma effects:	
	Earth's magnetic field	10
	S-, X-band beam mismatch	3
	Scintillations at low Sun angle	10
7	Relativity:	
	General Relativity	10
	Special Relativity	0–40
8	Numerical stability	2
	Estimates of total error	
1	Internal consistency:	
	Baseline repeatability	250
	Celestial pole repeatability	250
2	External consistency:	
	GSFC versus JPL radio frame	350
	ICRF versus JPL radio frame	300
3	Analyst choices	70–150

with DSS 15 and DSS 45 on March 22, 1992 (California–Australia), and DSS 15 and DSS 65 on March 27, 1992 (California–Spain), to test how well the JPL a priori group delay and phase rate models could be reproduced by independent software. After resolving some minor problems in all three codes, the final agreement amongst the codes was better than 1 ps in delay and 1 fs/s in phase delay rate over the 24-hour periods of the two experiments, based on comparison of several hundred delay–delay rate observable pairs. The largest unresolved discrepancy was due to differences between the implementations of the solid Earth tide model. Excluding these tidal differences, the JPL and GSFC softwares duplicated each other's calculations of relativistically corrected geometric delays to better than 0.1-ps rms, which translates to $\approx$1 μas in source position error for a 10,000-km baseline. Further details of this comparison are given in [49]. It is very unlikely that VLBI modeling software could be checked this carefully without

the existence of two or more independent programs. This validates the wisdom of the decision made two decades ago to develop independent VLBI software.

B. Same Data and Independent Software

In order to provide an external test of the accuracy of the JPL VLBI software implementation, a reference frame—designated 7893-185f—was generated using a subset of the JPL data (MkIII data from 1988–93) that had also been analyzed by the VLBI group at GSFC. Since both the JPL and GSFC groups started with the same data set, any differences in the resulting reference frames are due to a combination of differences in software implementation and analysts' choices in using the VLBI software of their respective institutions. The differences between the JPL and GSFC results are summarized in Table 10. Given the excellent agreement in the implementation of modeling software, it is apparent from the table that differences in analyst choices (parameterization of clocks and tropospheres, data editing, modeling options, etc.) can give rise to coordinate discrepancies at the level of 200 μas and rotational offsets at the level of 100 μas. Analyst choices for the full 1978–96 data set may be smaller due to averaging. The issue of the impact of analysts' choices is a difficult one to assess, largely because of the time and expense required to have an ensemble of analysts process a large data set using a complex model. Acknowledging such difficulties, we still feel that using the very limited test given above is preferable to an implicit assumption that all analysts' choices were optimally made.

Table 10. Comparison of the GSFC G915fh1 and JPL 7893-185f frames.

Item	Description	Value
1	Number of common sources	267
2	Median σ, μas	$\sigma_\alpha \cos\delta$, σ_δ,
	G-915fh1	170 270
	JPL 7893-185f	180 290
3	χ^2_ν	0.4
4	Rotation, μas	
	x	139 ± 25
	y	-13 ± 24
	z	-1 ± 17
5	Differences, μas	wrms, offset,
	$\Delta\alpha \cos\delta$	154 7
	$\Delta\delta$	207 20

C. Independent Data and Independent Software

As an additional assessment of the accuracy of the JPL reference frame, we have compared JPL source coordinates to a GSFC reference frame produced in the spring of 1997 based on data that GSFC and others had collected from 1979 to 1997; it is labeled G-1069. The GSFC catalog is based on independent data processed with independent software. This comparison is summarized in Table 11. Before differencing coordinates, a three-dimensional rotation was determined and removed in order to place the catalogs into best coincidence by eliminating any potential differences in JPL and GSFC frame orientation conventions, such as origin of right ascension and celestial ephemeris pole reference day (i.e., the day on which the nominal a priori precession/nutation model is used without adjustment). Since both catalogs were intentionally aligned to the new ICRF, one would expect the rotational offsets to be zero within the estimated errors. In fact they are. The estimated rotations about the x-, y-, and z-axes ($x, y = 0$ and 6 hr RA in the equatorial plane; z = spin axis) are 144 ± 42, -44 ± 47, and -8 ± 40 μas, respectively. The catalog differences give $\chi^2_\nu = 6.11 \pm 0.37$ for 533 degrees of freedom, indicating that the combined

Table 11. Comparison of the GSFC G-1069 and JPL 1997-3 frames.

Item	Description	Value
1	Number of common sources	268
2	Median σ, μas	$\sigma_\alpha \cos\delta$, σ_δ,
	GSFC G-1069	76 108
	JPL 1997-3	117 183
3	χ^2_ν	6.11 ± 0.37
4	Rotation, μas	
	x	144 ± 42
	y	-44 ± 47
	z	-8 ± 40
5	Differences, μas	wrms, offset,
	$\Delta\alpha \cos\delta$	315 66
	$\Delta\delta$	411 319

formal uncertainties underestimate the true errors by a factor of ≈2.5. We used the full covariances for both catalogs and assumed that JPL and GSFC error covariance matrices are independent. For the JPL catalog, which is based on the limited geometry provided by two DSN baselines, the off-diagonal elements of the full error covariance are important in determining the significance of zonal errors (e.g., $\Delta\delta$ versus δ).

Figure 7 shows the differences in source positions between the JPL 1997-3 and GSFC-1069 catalogs. As mentioned above, a three-dimensional rotation was removed prior to differencing in order to bring the catalogs into rotational alignment. Five large outliers also were removed from this comparison and are not plotted: P 0237−23, OI 417, P 2127+04, 3C 84, and P 2134+004. These sources are known to have non-point-like structures, and all but P 2134+004 required more than 100 ps of structure noise in our analysis (cf., Table 2), making them some of the worst sources for astrometry that we have observed. Thus, the comparison with the GSFC catalog provides independent confirmation of the usefulness of the source structure noise model represented by Tables 1 and 2. A least-squares estimate of the $\Delta\delta$ versus δ trend (see Fig. 7) was made. Although the effect is large (nearly 1 mas), it has a formal significance of only 2.9σ and a realistic significance about half that. This systematic trend in the differences is, therefore, more an indication of the geometric weakness of the JPL 1997-3 frame in the Southern Hemisphere than evidence of a statistically significant zonal error. This weakness was discussed earlier (Section V) in relation to large positive correlations amongst southern declinations. The importance of using the full source position covariance for the JPL reference frame is emphasized by a test that estimated the $\Delta\delta$ versus δ trend using only the diagonal elements of the source position covariance. In this case, the estimated declination trend is nearly three times larger and has a misleadingly large formal significance of 23σ! This result demonstrates that the full covariance information is essential for arriving at meaningful conclusions about the size and significance of zonal errors. In general, the GSFC covariance's off-diagonal elements are smaller than JPL's, presumably due to the more varied geometry of the data from multiple simultaneous baselines that were used to construct the GSFC catalog.

All of the preceding tests compare one VLBI frame to another VLBI frame. As such, these tests will not discover errors that are common to all users of the VLBI technique. It is desirable, therefore, to compare VLBI source positions with positions from another astrometric technique, such as the optical measurements from the European Space Agency's Hipparcos Satellite [73,25], which produced optical positions for ≈120,000 stars with accuracies near 1 mas. Lestrade et al. [56] have carried out a series of VLBI measurements to tie the radio-frequency positions of 12 of these stars to the positions of nearby

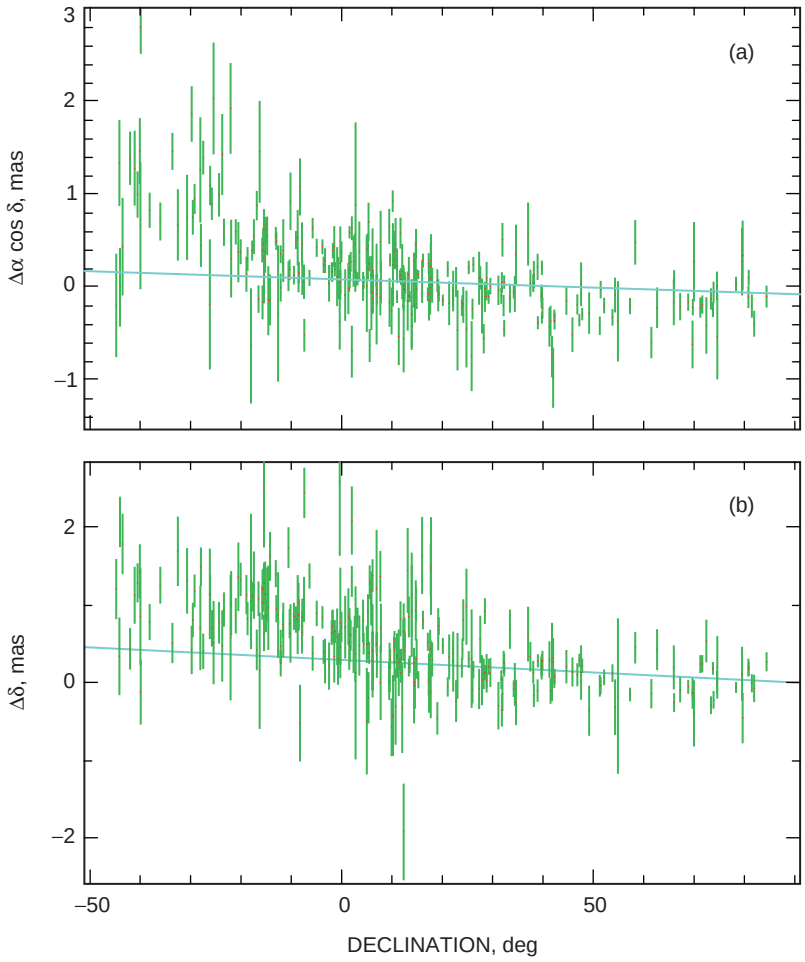

Fig. 7. Differences in source positions between the JPL 1997-3 and GSFC-1069 catalogs: (a) right ascension (arc length) differences versus declination and (b) declination differences versus declination. Note the systematic differences as a function of declination. These differences can be nearly 1 mas in the south. In particular, in Fig. 7(a), for $\Delta\alpha$ cos δ versus δ, the formal errors and the mean difference both increase in the region from δ = –20 to –50 deg, which can be observed only from one baseline, California–Australia. However, these differences have only marginal statistical significance because the JPL 1997-3 catalog used only one southern antenna, thereby weakening the southern geometry.

extragalactic radio sources. These ties verify that the Hipparcos optical technique and the VLBI radio technique are consistent with an accuracy of 1.7 mas in position and 0.84 mas/yr in proper motion [52], thereby increasing confidence that the VLBI astrometric results do not have large technique-dependent errors.

VIII. Comparison to the IAU Celestial Reference Frame

In August 1997, the IAU 23rd General Assembly voted to adopt a new fundamental reference frame based on VLBI measurements of extragalactic radio sources [47,64]. As of January 1, 1998, the VLBI-based International Celestial Reference Frame (ICRF) replaced the optically based Fundamental Katalog 5 (FK5) frame [31], which had systematic errors perhaps as large as 100 mas [69]. The ICRF analysis included about 80 percent of the 26,500 observations used in the JPL 1997-3 frame analysis plus more

than 1.6 million observations from other VLBI programs around the world. Consequently, the data used to construct these two frames are not completely independent. However, the analysis software used for the ICRF was Goddard's CALC/SOLV software, which is independent of JPL's MODEST software used to construct the 1997-3 frame. Thus, the comparison value of the JPL frame for the ICRF lies in its independent software, independent analyst choices, and partly independent data. Table 12 gives the differences between the JPL 1997-3 frame and the new ICRF. For the 202 sources that were in common, the wrms difference in $\alpha \cos\delta$ was 265 μas after the removal of a 34-μas mean difference. The wrms difference in δ was 344 μas after removal of a 271-μas mean difference. These results provide evidence that the new ICRF is accurate at the 300 μas level—almost 300 times better than the FK5 frame which it replaces! The accuracy of the ICRF is very important since all future astrometric work—be it radio frames, optical frames, or planetary ephemerides—will be based on the foundation provided by the ICRF. Thus, the verification of the ICRF provided by the JPL 1997-3 frame is important to a very wide range of astrometric efforts.

Table 12. Comparison of the ICRF and JPL 1997-3 frames.

Item	Description	Value
1	Number of common sources	202
2	Median σ, μas	$\sigma_\alpha \cos\delta$, σ_δ,
	ICRF	102 140
	JPL 1997-3	130 197
3	χ^2_ν	1.88 ± 0.13
4	Rotation, μas	
	x	-1 ± 68
	y	0 ± 69
	z	-12 ± 42
5	Differences, μas	wrms, offset,
	$\Delta\alpha \cos\delta$	265 34
	$\Delta\delta$	344 271

IX. Radio Frame Ties With the Planetary Ephemeris and Optical Frames

As we have just shown, the extragalactic radio frame is both very accurate and very stable. These qualities can benefit astrometric techniques in other frequency regimes and their associated reference frames if the appropriate links are made with the radio frame. For this reason, several experimental programs have been undertaken during the past decade in order to link both the planetary ephemeris frame and the Hipparcos optical frame to the extragalactic radio frame. In this section, we briefly review the results of efforts to make these ties using millisecond pulsars, planetary occultations of radio sources, spacecraft tracking, laser ranging, and VLBI measurements of radio stars.

A. Link to Planetary Ephemeris

The primary objective in linking the radio and planetary ephemeris frames is the desire to transfer the angular position of a spacecraft as measured by VLBI in the radio frame to the planetary ephemeris frame. Since the spacecraft target usually is some solar system body, it is necessary to make this connection from the spacecraft's radio frame position to the target's ephemeris frame position. Several techniques have been used to determine the relative orientation of the radio and ephemeris frames. These include observations of millisecond pulsars in both the radio frame and the ephemeris frame, timing the occultations of radio sources by planetary objects, and using spacecraft radio transmissions to obtain positions relative to

extragalactic radio sources, which then are compared with the corresponding ephemeris frame positions determined from the spacecraft orbit about the target body.

The time of arrival of pulsar signals is sensitive to the orbital motion of the Earth. Analysis of arrival time data yields the pulsar position relative to the Earth's orbit and thereby locates the pulsar in the ephemeris frame. Although there are various difficulties in detecting a pulsar signal using the VLBI technique, Bartel et al. [2], Dewey et al. [21], and Petit [74] have all been able to obtain results for the position of the millisecond pulsar PSR 1937+21 in the radio frame with an uncertainty of ≈5 mas.

Another method for deriving the radio–ephemeris frame tie is to time the epoch and duration of the occultation of a radio source by a solar system object. Roughly speaking, the mean epoch of the occultation is a measure of the ecliptic longitude, while the duration provides information concerning the ecliptic latitude of the occultation event. In [38], occultation by the Moon was used to measure the position of the radio source 3C 273 in the solar system ephemeris frame. Uncertainty in topography variations at the limb of the Moon limited the accuracy of the position to 200 mas. While this measurement is crude by current standards, the 3C 273 position obtained by lunar occultation served for more than a decade to define the fiducial point for determining right ascensions with VLBI. More recently, Linfield [58] used the occultation technique to measure the position of the radio source P 0507+17 relative to the orbit of Venus. The inferred frame tie in ecliptic longitude and latitude was estimated to be uncertain by ≈40 to 200 mas. The dense atmosphere of Venus makes it an unsuitable target for high-accuracy frame ties. Difficulty in calibrating the Venusian ionosphere was the primary source of error, dominating other smaller error sources, which were at the 10-mas level.

A third method for obtaining the radio–ephemeris frame tie involves fitting Doppler (phase rate) and range data from spacecraft radio transmissions with parameters that describe the spacecraft's orbit about the planet's center of mass (whose position is known from the ephemeris). This determination of the spacecraft's planet-relative position then is differenced with its radio frame position as obtained from differential range and Doppler measurements between extragalactic radio sources and the spacecraft transmissions. Newhall, Preston, and Esposito [70] initially used this technique on data from the Viking Mars and Pioneer Venus missions to obtain a link with an uncertainty of 20 mas. In [42], this type of analysis was performed on data from the Soviet Phobos spacecraft as it approached the Martian system. The authors obtained two of the three frame tie angles with an estimated accuracy of ≤8 mas. Another analysis of this type is in progress for data taken with the Magellan spacecraft at Venus, which has the potential to improve the frame tie accuracy to 1 mas.[10] Observations of the Mars Pathfinder spacecraft may provide yet another opportunity to improve the accuracy of the frame tie to ≈1 mas.[11] Link accuracies of 1 mas or better would start to be limited by systematic errors in the two frames being connected. Thus, improving the frame tie to better than 1-mas accuracy is likely to require improvements in the individual radio and ephemeris frames beyond their current accuracies. Such improvements will require critical analyses of a number of modeling defects at the submilliarcsecond level and are likely to involve several years of concentrated effort by researchers in space geodesy.

The last frame tie method we will discuss uses ground surveys between nearby VLBI, lunar laser ranging (LLR), and satellite laser ranging (SLR) stations to form a unified terrestrial frame. Offsets of the respective celestial frames then are estimated from differences in the Earth orientation parameters (UT1−UTC, polar motion, and celestial ephemeris pole longitude and obliquity) estimated from VLBI and LLR. This technique was used in [30] to measure offsets between the radio (VLBI) and ephemeris (LLR) celestial frames. The resulting tie has an estimated uncertainty of 3 mas in all three orthogonal rotation directions. Thus, the present accuracy of the tie between the radio and ephemeris frames is several times worse than the accuracy of either frame considered separately.

[10] W. M. Folkner, personal communication, Jet Propulsion Laboratory, Pasadena, California, 1997.

[11] E. M. Standish and W. M. Folkner, "The Latest Covariance of Mars," JPL Interoffice Memorandum 312.F-97-072 (internal document), Jet Propulsion Laboratory, Pasadena, California, December 25, 1997.

B. Link to Hipparcos Optical Frame

The Hipparcos optical catalog of ≈120,000 stars is characterized by position errors of ≈1 mas and proper motion errors of ≈1 mas/yr, with a mean epoch of observation of 1991.2. The Hipparcos optical catalog has been linked to the ICRF using about 12 extragalactic radio sources. The link accuracy is 600 μas in rotation angle and 250 μas/yr in rotation rate [56,52]. This tie allows optical and radio positions to be expressed in a consistent reference frame. We note in passing that the excellent results of the Hipparcos project were due in no small part to the use of two independent analysis teams. For future high-accuracy optical work, the extragalactic frame will provide a stable long-term reference system that could be used to calibrate the relatively uncertain proper motions of the Hipparcos catalog.

C. The Space Interferometry Mission

An ambitious space-based optical interferometer is now in the planning stages. It is called the Space Interferometry Mission (SIM) [http://huey.jpl.nasa.gov/sim/], and it is scheduled to launch in 2005. At present, the design calls for an optical interferometer with a 10-m baseline capable of determining a celestial reference frame of several thousand objects with a precision of 4 μas. This precision is almost two orders of magnitude better than the current state-of-the-art astrometry presented in this article. Furthermore, given sufficiently long integration time on a source, the SIM instrument is expected to be able to detect extragalactic radio sources (median magnitude $V \approx 18$) directly—a feat that was beyond Hipparcos's capabilities. Such observations would allow direct comparison of the radio and optical celestial frames at unprecedented levels of accuracy. Since the Hipparcos source positions are degrading by ≈1 mas/yr, they will have uncertainties of about 15 mas by the time SIM is launched. Thus, the VLBI radio frame will be the most accurate external standard available for verifying the SIM optical frame. Present VLBI accuracy is ≈50 times better than Hipparcos accuracy extrapolated to epoch 2005. If the troposphere errors discussed in this article can be overcome in the next 7 years, VLBI may increase this advantage to a factor of 100 or more. Thus, for the next decade, we anticipate that VLBI will continue to play a key role in improving the science of astrometry.

X. Conclusions

Deep Space Network VLBI measurements at 8.4 GHz (X-band) during the past two decades have culminated in the establishment of an accurate radio reference frame based on extragalactic radio source positions. The realistic accuracy of the JPL 1997-3 frame is ≈300 μas at epoch, with an overall frame stability of ≈50 μas/yr. The limiting error comes not from instrument sensitivity, but rather from inaccuracies in modeling the troposphere: primarily, mismodeled azimuthal asymmetries ("gradients") in atmospheric refractivity near the antenna, and to lesser extents inaccuracies in the model of the atmosphere's temperature at 2– to 10-km altitude and the signal's path delay through the turbulent layer of water vapor in the lower troposphere. Relatively few individual sources show statistically significant apparent proper motions at the 70-μas/yr level of our median rate uncertainty, indicating that structural evolution is not yet a dominant error. The utility of this frame has been extended through a tie to the JPL planetary ephemeris with an accuracy of ≈2 mas, and a tie to the Hipparcos optical frame to ≈600 μas in global orientation and 250 μas/yr in global rotation rate.

The JPL 1997-3 frame also is of central importance in assessing the systematic errors in the IAU's newly established International Celestial Reference Frame. Examination of the small discrepancies between the two frames has helped to reveal aspects of the VLBI technique that will require improvement in order to construct more accurate celestial frames in the future. This comparison was possible because the JPL program provided an independent source of VLBI data and analysis. Most importantly, the excellent agreement of the JPL 1997-3 frame and the ICRF provides assurance that the IAU's new fundamental frame is accurate at the submilliarcsecond level.

Acknowledgments

We appreciate the sustained assistance of Leroy Tanida, Lyle Skjerve, Jose Perea, and Pam Wolken in the acquisition of the DSN VLBI data over the years. Many others in the Tracking and Applications Section at JPL, as well as at the DSN stations, also contributed to both the data acquisition and data analysis during the past two decades. For access to the results of other celestial frame determinations, we thank Chopo Ma and Dave Gordon of the Goddard Space Flight Center and Marshall Eubanks of the U.S. Naval Observatory. For stimulating discussions and encouragement, we thank Leslie Morrison (present Chairman) and the IAU Working Group on Reference Frames. For an opportunity to visit the Paris Observatory to compare VLBI modeling software, C. S. Jacobs is grateful to Martine Feissel and Anne-Marie Gontier. For a very thorough critique of a draft of this article, we thank George Purcell.

References

[1] E. F. Arias, P. Charlot, M. Feissel, and J.-F. Lestrade, "The Extragalactic Reference System of the International Earth Rotation Service, ICRS," *A. & A.*, vol. 303, pp. 604–608, 1995.

[2] N. Bartel, J. F. Chandler, M. I. Ratner, I. I. Shapiro, R. Pan, and R. J. Cappallo, "Toward a Frame Tie Via Millisecond Pulsar VLBI," *Astron. J.*, vol. 112, no. 4, pp. 1690–1696, 1996.

[3] S. Bassiri and G. A. Hajj, "Higher Order Ionosphere Effects on the Global Positioning System Observables and Means of Modeling Them," *Manuscr. Geod.*, vol. 18, pp. 280–289, 1993.

[4] F. W. Bessel, "The Parallax of 61 Cygni," 1838, reprinted in *A Source Book in Astronomy*, eds. H. Shapley and H. Howarth, New York, p. 219, 1929.

[5] G. J. Bierman, *Factorization Methods for Discrete Sequential Estimation*, New York: Academic Press, 1977.

[6] J. G. Bolton, A. Savage, and A. E. Wright, "The Parkes 2700-MHz Survey—Part Fourteen—Catalogue and New Optical Identifications," *Australian J. of Physics*, vol. 46, p. 1, 1979.

[7] J. S. Border, F. F. Donivan, S. G. Finley, C. E. Hildebrand, B. Moultrie, and L. J. Skjerve, AIAA Paper 82-1471, presented at the 1982 AIAA Conference, San Diego, California, August 1982.

[8] J. Bradley, "An Account of a New Discovered Motion of the Fixed Stars," *Phil. Trans. Roy. Soc.*, vol. 35, p. 637, 1729. For a more accessible discussion, see A. B. Stewart, "The Discovery of Stellar Aberration," *Scientific American*, vol. 210, no. 3, pp. 100–108, March 1964.

[9] J. Bradley, "Concerning an Apparent Motion Observed in Some of the Fixed Stars", *Phil. Trans. Roy. Soc.*, vol. 45, pp. 1–43, 1748.

[10] P. Charlot, "Fourteen Extragalactic Radio Sources Mapped at 2.3 and 8.4 GHz With a 24-hour Crustal Dynamics Program VLBI Experiment," *A. & A.*, vol. 229, pp. 51–63, 1990.

[11] P. Charlot, "Evidence for Source Structure Effects Caused by the Quasar 3C 273 in Geodetic VLBI Data," in *VLBI Technology—Progress and Future Observational Possibilities, Proceedings of the URSI/IAU Symposium*, Kyoto Japan, September 6-10, 1993, eds. T. Sasao, S. Manabe, O. Kameya, and M. Inoue, pp. 287–294, Tokyo, Japan: Terra Scientific Publishing Company, 1994.

[12] P. Charlot, O. J. Sovers, J. G. Williams, and X X Newhall, "Precession and Nutation From Joint Analysis of Radio Interferometric and Lunar Laser Ranging Observations," *Astron. J.*, vol. 109, pp. 418–427, 1995.

[13] G. Chen and T. A. Herring, "Effects of Atmospheric Azimuthal Asymmetry on the Analysis of Space Geodetic Data," *J. Geophys. Res.*, vol. 102, no. B9, pp. 20,489–20,502, 1997.

[14] B. G. Clark, "The NRAO Tape-Recorder Interferometer System", *Proc. IEEE*, vol. 61, pp. 1242–1248, 1973.

[15] T. A. Clark, L. K. Hutton, G. E. Maradino, C. C. Counselman, D. S. Robertson, I. I. Shapiro, J. J. Wittels, H. F. Hinteregger, C. A. Knight, A. E. E. Rogers, A. R. Whitney, A. E. Niell, B. O. Rönnäng, and O. E. H. Rydbeck, "Radio Source Positions From Very Long Baseline Interferometry Observations," *Astron. J.*, vol. 81, no. 8, pp. 599–603, 1976.

[16] M. H. Cohen and D. B. Shaffer, *Astrophys. Let.*, vol. 76, p. 91, 1971.

[17] R. F. Coker, C. S. Jacobs, and L. E. Iriks, "VLBI DSN Flux Density Observations From 1989 to 1990 of 290 Extragalactic Radio Sources," *The Telecommunications and Data Acquisition Progress Repprt 42-131, July–September 1997*, Jet Propulsion Laboratory, Pasadena, California, pp. 1–25, November 15, 1997. http://tmo.jpl.nasa.gov/tmo/progress_report/42-131/131F.pdf

[18] A. E. Cole, A. Court, and A. J. Cantor, "Model Atmospheres," in *Handbook of Geophysics and Space Environments*, ed. S. L. Valley, New York: McGraw-Hill, p. 2-1, 1965.

[19] M. J. Crowe, *Modern Theories of the Universe from Herschel to Hubble*, New York: Dover Publications, pp. 26–27, 1994.

[20] C. DeMets, R. G. Gordon, D. F. Argus, and S. Stein, "Effect of Recent Revisions to the Geomagnetic Reversal Time Scale on Estimates of Current Plate Motions," *Geophys. Res. Let.*, vol. 21, pp. 2191–2194, 1994.

[21] R. J. Dewey, M. R. Ojeda, C. R. Gwinn, D. L. Jones, and M. M. Davis, "VLBI Astrometry of the Millisecond Pulsar B1937+21," *Astron. J.*, vol. 111, pp. 315–319, 1996.

[22] J. L. E. Dreyer, "New General Catalogue", *Mem. Roy. Astron. Soc.*, vol. 49, pp. 1–237, 1888. See also http://www.aspsky.org/html/resources/ngc.html

[23] J. L. E. Dreyer, "History of Astronomy From Thales to Kepler," 2nd ed. (unabridged republication of 1906 edition), New York: Dover Publications, 1953.

[24] D. O. Edge, J. R. Shakeshaft, W. B. McAdam, J. E. Baldwin, and S. Archer, "3rd Cambridge catalog," *Mem. Roy. Astron. Soc.*, vol. 68, p. 37, 1959.

[25] European Space Agency (ESA), *The Hipparcos and Tycho Catalogues*, Sci. Coord. M. A. C. Perryman, ESA SP-1200, 1997.

[26] F. W. Fallon and W. H. Dillinger, "Crustal Velocities From Geodetic Very Long Baseline Interferometry," *J. Geophys. Res.*, vol. 97, no. B5, pp. 7129–7136, 1992.

[27] J. L. Fanselow, O. J. Sovers, J. B. Thomas, E. J. Cohen, G. H. Purcell, Jr., D. H. Rogstad, L. J. Skjerve, and D. J. Spitzmesser, "Radio Interferometric Determination of Source Positions Utilizing Deep Space Network Antennas 1971–1980," *Astron. J.*, vol. 89, no. 7, pp. 987–998, 1984.

[28] A. L. Fey and P. Charlot, "VLBA Observations of Radio Reference Frame Sources, II. Astrometric Suitability Based on Observed Structure," *Astrophys. J. Suppl.*, vol. 111, pp. 95–142, 1997.

[29] A. L. Fey, A. W. Clegg, and E. B. Fomalant, "VLBA Observations of Radio Reference Frame Sources, I," *Astrophys. J. Suppl.*, vol. 105, pp. 299–330, 1996.

[30] W. M. Folkner, P. Charlot, M. H. Finger, J. G. Williams, O. J. Sovers, X X Newhall, and E. M. Standish, "Determination of the Extragalactic–Planetary Frame Tie From Joint Analysis of Radio Interferometric and Lunar Laser Ranging Measurements," *A. & A.*, vol. 287, pp. 279–289, 1994.

[31] W. Fricke, H. Schwan, T. Lederle, U. Bastian, R. Bien, G. Burkhardt, B. Dumont, R. Hering, R. Jaehrling, and H. Jahreiss, "The Fifth Fundamental Catalogue (FK5): Part 1, The Basic Fundamental Stars," Astronomische Rechen-Inst., Heidelberg, Germany, 1988.

[32] C. S. Gardner, "Correction of Laser Data for the Effects of Horizontal Refractivity Gradients," *Appl. Opt.*, vol. 16, no. 9, pp. 2427–2432, 1976.

[33] A.-M. Gontier, "Orientation de la Terre par Mesure VLBI," Ph.D. Dissertation, Observatory of Paris, Paris, France, 1992.

[34] P. W. Gorham, "Designing Optimal Bandwidth Synthesis Arrays for VLBI," *The Telecommunications and Mission Operations Progress Report 42-133, January–March 1998*, Jet Propulsion Laboratory, Pasadena, California, pp. 1–27, May 15, 1998.
http://tmo.jpl.nasa.gov/tmo/progress_report/42-133D.pdf

[35] R. S. Gross, summarized in the International Earth Rotation Service (IERS), *Annual Report for 1996*, Observatory of Paris, Paris, France, 1997.

[36] J. C. Guirado, J. M. Marcaide, A. Alberdi, P. Elosegui, M. I. Ratner, I. I. Shapiro, R. Kilger, F. Mantovani, T. Venturi, A. Rius, E. Ros, C. Trigilio, and A. R. Whitney, "Proper Motion of Components in 4C 39.25," *Astron. J.*, vol. 110, no. 6, pp. 2586–2596, 1995.

[37] E. Halley, "Considerations on the Change of the Latitudes of Some of the Principal Fixt Stars," *Philosophical Transactions of the Royal Society*, vol. 30, pp. 736-8, 1718. Reprinted in M. J. Crowe, *Modern Theories of the Universe from Herschel to Hubble*, New York: Dover Publications, pp. 22–24, 1994.

[38] C. Hazard, J. Sutton, A. N. Argue, C. M. Kenworthy, L. V. Morrison, and C. A. Murray, "Accurate Radio and Optical Positions of 3C 273B," *Nature*, vol. 233, pp. 89–91, 1971.

[39] T. A. Herring, "The ZMOA-1990 Nutation Series," in *Proceedings of the 127th Colloquium of the IAU: Reference Systems*, eds. J. A. Hughes, C. A. Smith, and G. H. Kaplan, U.S. Naval Observatory, Washington, D.C., pp. 157–166, 1991.

[40] T. A. Herring, J. L. Davis, and I. I. Shapiro, "Geodesy by Radio Interferometry: The Application of Kalman Filtering to the Analysis of VLBI Data," *J. Geophys. Res.*, vol. 95, pp. 12,561–12,582, 1990.

[41] J. F. W. Herschel, "Catalogue of Nebulae and Clusters of Stars," (a.k.a. "The General Catalogue"), *Phil. Trans. Roy. Soc.*, vol. 154, pp. 1–137, 1864.

[42] C. E. Hildebrand, B. A. Iijima, P. M. Kroger, W. M. Folkner, and C. D. Edwards, "Radio–Planetary Frame Tie From Phobos-2 VLBI Data," *The Telecommunications and Data Acquisition Progress Report 42-119, July–September 1994*, Jet Propulsion Laboratory, Pasadena, California, pp. 46–82, November 15, 1994. http://tmo.jpl.nasa.gov/tmo/progress_report/42-119/119C.pdf

[43] M. Hosokawa, K. Ohnishi, and T. Fukushima, "Fluctuation of Extragalactic Reference Frame Due to Gravitational Lensing in our Galaxy," *Astron. J.*, vol. 114, no. 4, pp. 1508–1516, 1997.

[44] E. P. Hubble, "Cepheids in Spiral Nebulae," *Popular Astronomy*, vol. 33, pp. 252–255, 1925. Reprinted in M. J. Crowe, *Modern Theories of the Universe From Herschel to Hubble*, New York: Dover Publications, pp. 331–335, 1994.

[45] E. P. Hubble, "A Relation Between Distance and Radial Velocity Among Extra-Galactic Nebulae," *Proc. Natl. Acad. Sci.*, vol. 15, pp. 168–173, 1929.

[46] International Earth Rotation Service (IERS), *Annual Report for 1994*, Observatory of Paris, Paris, France, 1995.

[47] International Astronomical Union (IAU), *The XXIIIrd General Assembly: Final Scientific Programme*, Kyoto, Japan, August 17–30, 1997.

[48] C. S. Jacobs, O. J. Sovers, J. G. Williams, and E. M. Standish, "The Extragalactic and Solar System Celestial Frames: Accuracy, Stability, and Interconnection," *Advances in Space Research*, vol. 13, pp. (11)161–174, 1993.

[49] C. S. Jacobs, O. J. Sovers, D. Gordon, C. Ma, and A.-M. Gontier, "The Accuracy of the ICRF: An Intercomparison of VLBI Analysis Software," Joint Discussion #7, XXIIIrd IAU General Assembly, Kyoto, Japan, August 1997. To appear in *Highlights in Astronomy*, Dordrecht: Kluwer, 1998.

[50] K. G. Jansky, "Radio Waves From Outside the Solar System", *Nature*, vol. 132, p. 66, 1933. See also K. G. Jansky, *Proc. IRE*, vol. 20, p. 1920, 1932.

[51] K. J. Johnston, A. L. Fey, N. Zacharias, J. L. Russell, C. Ma, C. de Vegt, D. L. Jauncey, J. E. Reynolds, B. A. Archinal, M. S. Carter, T. E. Corbin, T. M. Eubanks, D. R. Florkowski, D. M. Hall, D. D. McCarthy, P. M. McCulloch, G. D. Nicolson, and D. B. Shaffer, "A Radio Reference Frame," *Astron. J.*, vol. 110, p. 880, 1995.

[52] J. Kovalevsky, L. Lindegren, M. A. C. Perryman, P. D. Hemenway, K. J. Johnston, V. S. Kislyuk, J. F. Lestrade, L. V. Morrison, I. Platais, S. Roser, E. Schilbach, H.-J. Tucholke, C. de Vegt, J. Vondrak, F. Arias, A.-M. Gontier, F. Arenou, P. Brosche, D. R. Florkowski, S. T. Garrington, R. A. Preston, C. Ron, S. P. Rybka, R.-D. Scholz, and N. Zacharias, "The Hipparcos Catalogue as a Realization of the Extragalactic Reference System," *A. & A.*, vol. 323, pp. 620–633, 1997.

[53] G. E. Lanyi, "Tropospheric Delay Effects in Radio Interferometry," *The Telecommunications and Data Acquisition Progress Report 42-78, April–June 1984*, Jet Propulsion Laboratory, Pasadena, California, pp. 152–159, August 15, 1984.

[54] H. Leavitt, "Periods of 25 Variable Stars in the Small Magellanic Cloud," *Harvard College Observatory Circular*, no. 173, Harvard University, Cambridge, Massachusetts, pp. 1-3, March 3, 1912.

[55] D. E. Lebach, B. E. Corey, I. I. Shapiro, M. I. Ratner, J. C. Webber, A. E. E. Rogers, J. L. Davis, and T. A. Herring, "Measurement of the Solar Gravitational

Deflection of Radio Waves Using Very Long Baseline Interferometry," *Phys. Rev. Let.*, vol. 75, no. 8, pp. 1439–1442, 1995.

[56] J.-F. Lestrade, D. L. Jones, R. A. Preston, R. B. Phillips, M. A. Titus, J. Kovalevsky, L. Lindegren, R. Hering, M. Froeschle, J. L. Falin, F. Mignard, C. S. Jacobs, O. J. Sovers, T. M. Eubanks, and D. Gabuzda, "Preliminary Link of the Hipparcos and VLBI Reference Frames," *A. & A.*, vol. 304, pp. 182–188, 1995.

[57] J. H. Lieske, T. Lederle, W. Fricke, and B. Morando, "Expressions for the Precession Quantities Based Upon the IAU 1976 System of Astronomical Constants," *A. & A.*, vol. 58, no. 1, pp. 1–16, 1977.

[58] R. P. Linfield, "Occultation of a Compact Radio Source by Venus," *Astron. J.*, vol. 104, pp. 880–890, 1992.

[59] S. T. Lowe, *Theory of Post-Block II VLBI Observable Extraction*, JPL Publication 92-7, Jet Propulsion Laboratory, Pasadena, California, July 15, 1992.

[60] C. Ma, "Very Long Baseline Interferometry Applied to Polar Motion, Relativity and Geodesy," Ph.D. Dissertation, University of Maryland; also NASA TM 79582, Goddard Space Flight Center, Greenbelt, Maryland, 1978.

[61] C. Ma, "Extragalactic Reference Frames," in *Reference Frames in Astronomy and Geophysics*, eds. J. Kovalevsky, I. I. Mueller, and B. Kolaczek, Astrophysics and Space Science Library, vol. 154, Dordrecht: Kluwer, pp. 43–65, 1989.

[62] C. Ma, D. B. Schaffer, C. de Vegt, K. J. Johnston, and J. L. Russell, "A Radio Optical Reference Frame, I. Precise Radio Source Positions Determined by Mark III VLBI: Observations From 1979 to 1988 and a Tie to the FK5," *Astron. J.*, vol. 99, pp. 1284–1298, 1990.

[63] C. Ma, E. F. Arias, T. M. Eubanks, A. L. Fey, A.-M. Gontier, C. S. Jacobs, O. J. Sovers, B. A. Archinal, and P. Charlot, in *IERS Technical Note 23*, eds. C. Ma and M. Feissel, Observatory of Paris, Paris, France, 1997.

[64] C. Ma, E. F. Arias, T. M. Eubanks, A. L. Fey, A.-M. Gontier, C. S. Jacobs, O. J. Sovers, B. A. Archinal, and P. Charlot, "The International Celestial Reference Frame Based on VLBI Observations of Extragalactic Radio Sources,", *Astron. J.*, in press, to appear July 1998.

[65] D. S. MacMillan and C. Ma, "Atmospheric Gradients and the VLBI Terrestrial and Celestial Reference Frames," *Geophys. Res. Lett.*, vol. 24, no. 4, pp. 453–456, 1997.

[66] D. D. McCarthy, ed., *IERS Conventions, IERS Technical Note 21*, International Earth Rotation Service, Observatory of Paris, Paris, France, 1996.

[67] C. Messier, "Catalogue of Nebulae and Star Clusters," 1781, in *Connaissance des Temps* for 1784. See also http://www.seds.org/messier or J. H. Robinson and J. Muirden, *Astronomy Data Book*, New York: Wiley, 1979.

[68] J. M. Moran, "Spectral-Line Analysis of Very Long Baseline Interferometric Data," *Proc. IEEE*, vol. 61, pp. 1236–1242, 1973.

[69] L. V. Morrison, P. Gibbs, L. Helman, C. Fabricus, and O. Einicke, "Evidence of Systematic Errors in FK5," *Astrophysics and Space Science*, vol. 177, nos. 1–2, pp. 31–34, 1991.

[70] X X Newhall, R. A. Preston, and P. B. Esposito, "Relating the JPL VLBI Reference Frame and the Planetary Ephemeris," in *Astrometric Techniques, Proceedings of IAU Symposium 109*, eds. H. K. Eichhorn and R. J. Leacock, Dordrecht: Reidel, pp. 789–794, 1986.

[71] A. E. Niell, "Global Mapping Functions for the Atmosphere Delay at Radio Wavelengths," *J. Geophys. Res.*, vol. 101, pp. 3227–3246, 1996.

[72] A. Patnaik, I. W. A. Browne, P. N. Wilkinson, and J. M. Wrobel, "Interferometer Phase Calibration Sources, I—The Region 35–75 deg," *Mon. Not. Roy. Ast. Soc.*, vol. 254, pp. 655–676, 1992.

[73] M. A. C. Perryman, "Hipparcos—Astrometry From Space," *Nature*, vol. 340, no. 6229, p. 111, 1989.

[74] G. Petit, "Observations VLBI des Pulsars Millisecondes Pour le Raccordement des Systèmes de Référence Célestes et la Stabilité des Échelles de Temps", Ph.D. Dissertation, Observatory of Paris, Paris, France, 1994.

[75] T. Pyne, C. R. Gwinn, M. Birkinshaw, T. M. Eubanks, and D. N. Matsakis, "Gravitational Radiation and Very Long Baseline Interferometry," *Astrophys. J.*, vol. 465, p. 566, 1996.

[76] G. Reber, "Cosmic Static," *Astrophys. J.*, vol. 91, pp. 621–624, 1940.

[77] G. Reber, "Cosmic Static," *Astrophys. J.*, vol. 100, pp. 279–287, 1944.

[78] M. J. Rees, "Black Hole Models for Active Galactic Nuclei," *Annual Review of Astronomy and Astrophysics*, vol. 22, pp. 471–506, 1984.

[79] D. S. Robertson, "Geodetic and Astrometric Measurements With Very Long Baseline Interferometry," Ph.D. Dissertation, Massachusetts Institute of Technology; also NASA X922-77-228, Goddard Space Flight Center, Greenbelt, Maryland, 1975.

[80] D. S. Robertson, F. W. Fallon, and W. E. Carter, "Celestial Reference Coordinate Systems—Sub-milliarcsecond Precision Demonstrated With VLBI Observations," *Astron. J.*, vol. 91, p. 1456, 1986.

[81] D. S. Robertson, W. E. Carter, and W. H. Dillinger, "New Measurement of Solar Gravitational Deflection of Radio Signals Using VLBI," *Nature*, vol. 349, pp. 768–770, 1991.

[82] A. E. E. Rogers, "Very Long Baseline Interferometry With Large Effective Bandwidth for Phase-Delay Measurements," *Radio Science*, vol. 5, no. 10, pp. 1239–1247, 1970.

[83] A. E. E. Rogers, "A Receiver Phase and Group Delay Calibrator for Use in Very Long Baseline Interferometry," Haystack Observatory Technical Note 1975-6, Haystack Observatory, Westford, Massachusetts, 1975.

[84] A. E. E. Rogers, R. J. Cappalo, H. F. Hinteregger, J. I. Levine, E. F. Nesman, J. C. Webber, A. R. Whitney, T. A. Clark, C. Ma, J. Ryan, B. E. Corey, C. C. Counselman, T. A. Herring, I. I. Shapiro, C. A. Knight, D. B. Shaffer, N. R. Vandenberg, R. Lacasse, R. Mauzy, B. Rayhrer, B. R. Schupler, and J. C. Pigg, "Very-Long-Baseline Interferometry: The MkIII System for Geodesy, Astrometry and Aperture Synthesis," *Science*, vol. 219, p. 51, 1983.

[85] J. L. Russell, D. L. Jauncey, B. R. Harvey, G. L. White, J. E. Reynolds, C. Ma, K. J. Johnston, A. Nothnagel, G. Nicolson, K. Kingham, R. Hindsley, C. de Vegt, N. Zacharias, and D. F. Malin, "A Radio Optical Reference Frame, III. Additional Radio and Optical Positions in the Southern Hemisphere", *Astron. J.*, vol. 103, pp. 2090–2098, 1992.

[86] P. K. Seidelmann, "1980 IAU Theory of Nutation: The Final Report of the IAU Working Group on Nutation," *Celestial Mechanics*, vol. 27, pp. 79–106, 1982.

[87] E. H. Sigman, "Phase Calibration Generator", *The Telecommunications and Data Acquisition Progress Report 42-92, October–December 1987*, Jet Propulsion Laboratory, Pasadena, California, pp. 86–104, February 15, 1988.

[88] O. J. Sovers, C. D. Edwards, C. S. Jacobs, G. E. Lanyi, K. M. Liewer, and R. N. Treuhaft, "Astrometric Results of 1978–1985 Deep Space Network Interferometry: The JPL 1987-1 Extragalactic Source Catalog," *Astron. J.*, vol. 95, pp. 1647–1658, 1988.

[89] O. J. Sovers, C. S. Jacobs, and R. S. Gross, "Measuring Rapid Ocean Tidal Earth Orientation Variations With VLBI," *J. Geophys. Res.*, vol. 98, pp. 19,959–19,971, 1993.

[90] O. J. Sovers and C. S. Jacobs, *Observation Model and Parameter Partials for the JPL VLBI Parameter Estimation Software "MODEST"–1996*, JPL Publication 83-39, Rev. 6, Jet Propulsion Laboratory, Pasadena, California, August 1996.

[91] O. J. Sovers, J. L. Fanselow, and C. S. Jacobs, "Astrometry and Geodesy With Radio Interferometry: Experiments, Models, Results," *Rev. Mod. Phys.*, vol. 70, October 1998.

[92] E. M. Standish and X X Newhall, "New Accuracy Levels for Solar System Ephemerides," in *Proceedings of IAU Symp. 172—Dynamics, Ephemerides, and Astrometry of the Solar System*, eds. S. Ferraz-Mello et al., Dordrecht: Kluwer, pp. 29–36, 1996.

[93] L. P. Teitelbaum, S. J. Keihm, R. P. Linfield, M. J. Mahoney, and G. M. Resch, "A Demonstration of Precise Calibration of Tropospheric Delay Fluctuations With Water Vapor Radiometers," *Geophys. Res. Letters*, vol. 23, no. 25, pp. 3719–3722, 1996.

[94] J. B. Thomas, "The Tone Generator and Phase Calibration in VLBI Measurements," *Deep Space Network Progress Report 42-44*, Jet Propulsion Laboratory, Pasadena, California, pp. 63–74, January 1978.

[95] J. B. Thomas, *An Analysis of Radio Interferometry With the Block 0 System*, JPL Publication 81-49, Appendix F, Jet Propulsion Laboratory, Pasadena, California, December 15,1981.

[96] J. B. Thomas, *Interferometry Theory for the Block II Processor*, JPL Publication 87-29, Jet Propulsion Laboratory, Pasadena, California, October 15, 1987.

[97] D. M. Tralli and S. M. Lichten, "Stochastic Estimation of Tropospheric Path Delays in Global Positioning System Geodetic Measurements," *Bulletin Geodesique*, vol. 64, pp. 127–159, 1990.

[98] R. N. Treuhaft and G. E. Lanyi, "The Effect of the Dynamic Wet Troposphere on Radio Interferometric Measurements," *Radio Science*, vol. 22, pp. 251–265, 1987.

[99] R. N. Treuhaft and S. T. Lowe, "A Measurement of Planetary Relativistic Deflection," *Astron. J.*, vol. 102, pp. 1879–1888, 1991.

[100] C. M. Wade and K. J. Johnston, "Precise Positions of Radio Sources, V. Positions of 36 Sources Measured on a Baseline of 35 km," *Astron. J.*, vol. 82, no. 10, pp. 791–795, 1977.

[101] J. M. Wahr, "The Forced Nutations of an Elliptical, Rotating, Elastic, and Oceanless Earth," *Geophys. J. Roy. Astron. Soc.*, vol. 64, pp. 705–727, 1981.